# Applied Research Laboratory



## Technical Report

**DISCRETE-FREQUENCY RADIATED NOISE AND UNSTEADY ROTOR FORCE FROM A SUBSONIC AXIAL FLOW FAN**

by

Wen-Shyang Chiu
G. C. Lauchle
D. E. Thompson



PENNSTATE

4

The Pennsylvania State University
**APPLIED RESEARCH LABORATORY**
P. O. Box 30
State College, PA 16804

# DISCRETE-FREQUENCY RADIATED NOISE AND UNSTEADY ROTOR FORCE FROM A SUBSONIC AXIAL FLOW FAN

by

Wen-Shyang Chiu
G. C. Lauchle
D. E. Thompson

Technical Report No. TR 88-009

July 1988



Supported by:
Naval Sea Systems Command

L. R. Hettche, Director
Applied Research Laboratory

Unclassified
SECURITY CLASSIFICATION OF THIS PAGE

# REPORT DOCUMENTATION PAGE

| | |
|---|---|
| 1a REPORT SECURITY CLASSIFICATION<br>Unclassified | 1b. RESTRICTIVE MARKINGS |
| 2a SECURITY CLASSIFICATION AUTHORITY | 3 DISTRIBUTION / AVAILABILITY OF REPORT<br>Unlimited |
| 2b DECLASSIFICATION / DOWNGRADING SCHEDULE | |
| 4 PERFORMING ORGANIZATION REPORT NUMBER(S) | 5. MONITORING ORGANIZATION REPORT NUMBER(S) |
| 6a NAME OF PERFORMING ORGANIZATION<br>Applied Research Laboratory<br>The Pennsylvania State University<br>6b OFFICE SYMBOL (If applicable)<br>ARL | 7a. NAME OF MONITORING ORGANIZATION |
| 6c ADDRESS (City, State, and ZIP Code)<br>P. O. Box 30<br>State College, PA 16804 | 7b. ADDRESS (City, State, and ZIP Code) |
| 8a NAME OF FUNDING / SPONSORING ORGANIZATION<br>International Business Machines<br>8b OFFICE SYMBOL (If applicable)<br>IBM | 9. PROCUREMENT INSTRUMENT IDENTIFICATION NUMBER |
| 8c ADDRESS (City, State, and ZIP Code)<br>3605 Highway 52N<br>Rochester, MN 55901 | 10. SOURCE OF FUNDING NUMBERS<br>PROGRAM ELEMENT NO. / PROJECT NO. / TASK NO. / WORK UNIT ACCESSION NO. |

11 TITLE (Include Security Classification)
Discrete-Frequency Radiated Noise and Unsteady Rotor Force from a Subsonic Axial Flow Fan

12 PERSONAL AUTHOR(S)
Wen-Shyang Chiu, G. C. Lauchle, D. E. Thompson

| 13a TYPE OF REPORT | 13b TIME COVERED | 14. DATE OF REPORT (Year, Month, Day) | 15. PAGE COUNT |
|---|---|---|---|
| M.S. Thesis | FROM _____ TO _____ | July 1988 | 98 |

16 SUPPLEMENTARY NOTATION

| 17 COSATI CODES | | | 18 SUBJECT TERMS (Continue on reverse if necessary and identify by block number) |
|---|---|---|---|
| FIELD | GROUP | SUB-GROUP | acoustic field, acoustic variables measurement, acoustic waves, two phase fluid flow, unsteady force fields |
| | | | |
| | | | |

19 ABSTRACT (Continue on reverse if necessary and identify by block number)

The noise radiated by a subsonic, axial-flow fan at its rotational frequency and harmonics is related to the non-steady force field created at the rotor blade/fluid interface. This force field is highly dependent on the time-invariant flow distortions that enter the fan. In this basic study, a typical cooling fan used in the electronic and computer industry was instrumented with a shaft unsteady axial force

| | |
|---|---|
| 20 DISTRIBUTION / AVAILABILITY OF ABSTRACT<br>☒ UNCLASSIFIED/UNLIMITED ☐ SAME AS RPT ☐ DTIC USERS | 21. ABSTRACT SECURITY CLASSIFICATION |
| 22a NAME OF RESPONSIBLE INDIVIDUAL | 22b. TELEPHONE (Include Area Code) / 22c. OFFICE SYMBOL |

DD FORM 1473, 84 MAR — 83 APR edition may be used until exhausted. All other editions are obsolete.

SECURITY CLASSIFICATION OF THIS PAGE
Unclassified

sensor. Its output is proportional to the total unsteady axial force created by the rotor. The on-axis sound pressure levels were measured and compared to coherent output power spectra involving the unsteady force sensor and the microphone. Very good coherence at the discrete tones is observed.

The inflow field of the fan was systematically distorted by placing a small cylinder at various positions in the inlet plane. The non-uniform, three-dimensional flow field entering the rotor was measured by traversing a set of miniature five-hole pressure probes. The total pressure outputs from this probe can be related to the axial, tangential, and radial velocity vectors. Fourier decomposition of the inflow velocity data is coupled with analysis to give information on the unsteady rotor force harmonic content. A simplified Curle's equation was then used to compute the discrete-frequency radiated noise at the Blade Passage Frequency (BPF) and its harmonics. The predicted and measured noise levels are in close agreement at the BPF and the first harmonic when the fan is a compact source.

The fan inlet and fingerguard of the test fan were modified and evaluated acoustically. Evaluation shows that the addition of a baffle does not reduce the fan noise. It is desirable that the radial members of the finger guard cross the blade leading edge at a large angle and pass by only a small portion of the blade leading edge at any instant of time. The unsteady blade force and thus the discrete-frequency radiated noise will be reduced.

# ABSTRACT

The noise radiated by a subsonic, axial-flow fan at its rotational frequency and harmonics is related to the non-steady force field created at the rotor blade/fluid interface. This force field is highly dependent on the time-invariant flow distortions that enter the fan. In this basic study, a typical cooling fan used in the electronic and computer industry was instrumented with a shaft unsteady axial force sensor. Its output is proportional to the total unsteady axial force created by the rotor. The on-axis sound pressure levels were measured and compared to coherent output power spectra involving the unsteady force sensor and the microphone. Very good coherence at the discrete tones is observed.

The inflow field of the fan was systematically distorted by placing a small cylinder at various positions in the inlet plane. The non-uniform, three-dimensional flow field entering the rotor was measured by traversing a set of miniature five-hole pressure probes. The total pressure outputs from this probe can be related to the axial, tangential, and radial velocity vectors. Fourier decomposition of the inflow velocity data is coupled with analysis to give information on the unsteady rotor force harmonic content. A simplified Curle's equation was then used to compute the discrete-frequency radiated noise at the Blade Passage Frequency (BPF) and its harmonics. The predicted and measured noise levels are in close agreement at the BPF and the first harmonic when the fan is a compact source.

The fan inlet and fingerguard of the test fan were modified and evaluated acoustically. Evaluation shows that the addition of a baffle does not reduce the fan noise. It is desirable that the radial members of the finger guard cross the blade leading edge at a large angle and

pass by only a small portion of the blade leading edge at any instant of time. The unsteady blade force and thus the discrete-frequency radiated noise will be reduced.

TABLE OF CONTENTS

TABLE OF CONTENTS (continued)

# LIST OF TABLES

# LIST OF FIGURES

LIST OF FIGURES (Continued)

LIST OF FIGURES (Continued)

# ACKNOWLEDGEMENTS

I would like to express sincere thanks to my thesis advisors, Dr. Gerald C. Lauchle and Dr. Donald E. Thompson, for their advice and encouragement throughout this research. I also wish to thank Mr. Allen L. Treaster, Mr. Neil B. Kimerer, Jr. and Mr. James H. Prout for help with the experimental setup, Mr. William C. Zierke for assistance with computer programs, and Mr. Karl Grosh for force transducer design. The experimental investigation could not have been carried out without the generous help extended by the Water Tunnel crew. I would especially like to thank my wife, Yia-Shun Yen, for her love and encouragement during my education.

This project was done at the Applied Research Laboratory of The Pennsylvania State University under contract with IBM Corp. Their support is gratefully acknowledged.

# Chapter 1

# INTRODUCTION

## 1.1 Axial Fan Noise Mechanism

The noise sources of a small axial-flow cooling fan include aerodynamic, mechanical and electromagnetic sources. The primary sources of mechanical noise are bearing noise and rotor unbalance. The magnetic noise is caused by the motor which drives the rotor. The aerodynamic noise source, which is caused mainly by the viscous flow over the blades and the interaction between blades and inflow disturbances, is the principal noise source of an axial-flow fan.

The acoustic spectrum of aerodynamic noise is characterized by a broadband component and a series of discrete-frequency peaks related to the Blade Passage Frequency (BPF) which is equal to the number of blades multiplied by the revolutions per second of the rotor. The major broadband noise sources include the blade vortex shedding from the blade trailing edge, blade to blade vortex interaction, laminar flow separation on the suction surface, and random fluctuating blade forces caused by the blade boundary layer and interaction with inflow turbulence [1,2,3,4]. The discrete-frequency noise mechanisms are a result of fluctuating blade forces which are caused by the interaction of the blades and non-uniform inflow [5,6,7,8]. It is the discrete-frequency noise that is usually regarded as being psychologically disturbing [9].

The inflow velocity disturbance of a fan may be of two origins: upstream wakes from an obstruction placed near the fan inlet or from

the stretching of large-scale eddies into vortices as they are drawn into the potential sink of the fan [5]. This latter mechanism often time averages out over long time observation; hence, the dominating discrete tone sources are caused by the interaction between obstruction wakes and blades. As a blade passes through an obstruction wake, it experiences a velocity change and an unsteady lift due to the resulting change in angle of attack. The unsteady aerodynamic force acting on the rigid blade will cause a fluctuating pressure field. In air, which is a compressible medium, the pressure fluctuation in the field will radiate as a dipole sound source. If the unsteady force is spatially r petitive for each rotor revolution, it can be Fourier analyzed into sinusoidal blade loading harmonics, together with their appropriate phase relationships. These components generate a set of rotating modes, and each mode radiates discrete-frequency sound in its corresponding radiation pattern.

There have been numerous research studies on the mechanism of discrete-frequency blade noise [10,11,12,13,14]. Ribner and Clark [12] substantiated the Curle theory by demonstrating a direct relationship between the fluctuating lift on an airfoil and the resulting far-field acoustic pressure. Hersh, Meechan and Bies [13] reconfirmed that the small airfoils exhibit a dipole directivity. Baade [10] showed that the noise at the BPF is primarily a dipole source. Wright [11,14] found that the fluctuating forces on rotating blades, i.e., rotating acoustic dipoles, are the principle sources for discrete-frequency noise. He found also that the steady blade force produces little radiation compared with the fluctuating blade force. Efficient

discrete-frequency noise requires only a small amount of fluctuating force [15]. Significant discrete-frequency noise can be caused by a fluctuating blade force as small as one one-thousandth of the steady-state blade loading.

## 1.2 Research Background

In 1981-82, the IBM Corporation began support of a research program at the Applied Research Laboratory of The Pennsylvania State University (ARL/PSU) directed toward the identification and reduction of discrete-frequency noise sources in small axial flow cooling fans such as those which can be found in electronic equipment. Four (4) Rotron fans were provided for an experimental evaluation and modification (Tarzan, Muffin, Muffin XL, and Patriot) performed by Fitzgerald [16,17]. He used an unobstructed inflow for the fans and found that the shroud support struts, casing, and other asymmetries associated with the fan itself cause tonal radiation at harmonics of the blade-passage frequency. It was shown that the tonal energy could be reduced by streamlining the support struts, by adding bellmouths to the inlet end of the shroud, and by incorporating flow modifiers to the rotor blades, among others.

The modifications recommended by Fitzgerald [16] may not always produce the noise reductions quoted when the fan is operated in practice. For example, when mounted in a cabinet for cooling purposes, the inflow will more than likely be quite disturbed, realizing that it must pass through louvers as well as being affected by cabinet

boundaries and the floor and walls of the rooms where the cabinet is situated. For this reason, a second laboratory investigation was carried out in 1983-85. In this second phase, Washburn [18] conducted a very systematic study of the tonal radiation from the Muffin XL and Tarzan fan models. He introduced idealized inflow disturbances created by stationary objects. These objects included a circular cylinder in cross flow, a rectangular cylinder, rectangular plates that block a large percentage of the inflow, and card gate models. As expected, the fan improvements suggested by Fitzgerald lost their noise reduction effectiveness when the inflow was disturbed by these objects. Washburn postulated that the harmonics of the BPF were a result of the unsteady rotor blade loading induced by the spatially periodic inflow distortions.

Washburn's design recommendations include the aerodynamic shaping of unavoidable inflow obstructions, the identification of a minimum distance of 0.3 fan radii for the placement of such obstructions, the avoidance of any sort of blockage in the lateral inflow, and the possible use of inlet baffles that help accelerate the flow and hence reduce the distortion field.

It was not within the scope of Washburn's Master of Science program to continue investigation of these recommendations. Such continuation entails the fabrication and evaluation of the recommended devices. Also, the design requires a detailed knowledge of the time random and mean velocity vectors at the inlet of the fan. The acquisition of these aerodynamic data, the inlet re-design and acoustic evaluation of prototype configurations, will require a third phase of this overall

fan noise reduction effort. It is this third phase that is studied here.

## 1.3 Research Objectives

The overall objective of this research is to provide means for the reduction of the harmonics of the BPF radiated sound through inflow ducting re-design. Specific sub-objectives include: (1) quantitative correlation of non-steady blade lift to radiated sound at the BPF and its harmonics; (2) quantitative measurements of the spatial distribution of time invariant inflow velocity vectors; and (3) design and evaluation of modified duct inlet and finger guard configurations.

## 1.4 Approach

The blade unsteady lift is due primarily to operation in time invariant inflow non-uniformities. In order to reduce the blade unsteady forces and resulting radiated sound, the rotor non-uniform inflow fields typical of fan operation must be quantified. For the typical obstructions considered in this investigation, measurements of the spatial non-uniform inflow fields to the rotor will be made using miniature five-hole pressure probes. Fourier analysis of the circumferential variation of the spatial non-uniformities will be performed, resulting in input for inlet re-design to reduce unsteady lift and resulting BPF and multiple radiated noise. Spatial variations of the non-uniformities will be used to assess the blade unsteady lift

due to this source and to reduce this effect and the resulting radiated sound.

Based on the objectives set forth, it will be necessary to equip the selected fan with an internal sensor. For ease in sensor installation and enhancement of blade signals from these sensors, the Patriot fan was selected for detailed aeroacoustic study.

To measure non-steady blade loading, the motor shaft housing of the Patriot will be modified and a piezo-ceramic disk will be incorporated. This crystal will, in effect, sense the total unsteady rotor axial force. The complex coherence function and the coherent output power spectrum between measured shaft force and radiated sound pressure will be used to determine the acoustic pressure at the microphone due to the fluctuating force on the rotor. This procedure will be performed with and without the cylindrical inflow obstruction studies previously by Washburn [18].

In addition, modified duct inlets and finger guards will be designed and tested. The purpose is to reduce the interaction noise caused by the finger guards, to smooth the inflow surrounding the shroud inlet, and thus to reduce discrete-frequency noise.

# Chapter 2

# CORRELATION OF DISCRETE FREQUENCY NOISE AND UNSTEADY ROTOR FORCE

## 2.1 Introduction

The major discrete-frequency noise sources include the steady blade loading, which contributes to the noise at the BPF, and the periodic unsteady loading, which contributes to the noise at the BPF and its harmonics. The periodic unsteady loading is caused mainly by the interaction of the fan blades with the time-invariant non-uniform inflow. This results in the blades radiating sound as a dipole source on the fan axis. In order to correlate the unsteady rotor force to the discrete-frequency noise, two test conditions are required. One condition is a fan without any obstruction. The other condition is a fan with some generic obstruction positioned in front of the center of the fan. A 1.27 cm diameter cylinder is used for this generic obstruction. the cylinder generates two cycles of inflow distortion per rotor revolution. The diameter of the Patriot fan is about 18 cm [19]. During the tests, described below, the fan was operated at the minimum static pressure rise condition in order to maximize the discrete-frequency noise [16,17,18]. The coherent output power spectrum and the coherence function for the unsteady rotor force and the fan noise were used to indicate the contribution of the unsteady

loading to the fan noise. Experimental results are presented and discussed.

## 2.2 Experimental Setup

The measurements of unsteady rotor force and fan noise were conducted in an "air-breathing" anechoic chamber, where the air can flow into the chamber through acoustically-treated air passages. The fan exhausts the air out of the chamber through an acoustic duct. Figure 2.1 shows a schematic of the test facility assembly. There is an anechoic termination and throttle located at the duct outlet. The anechoic termination was used to reduce the formation of longitudinal standing waves within the duct. The throttle was used to regulate the static pressure and air flow. The duct was lined with sound and vibration insulation material to attenuate the vibration and sound generated by the test fan. The material effectively damped the transverse standing waves within the duct. The duct inlet was positioned 120 cm within the chamber to minimize the interaction of inflow distortions generated by the foam wedges attached to the chamber walls. A B&K type 4220 2.54 cm microphone was positioned on the fan axis at a distance 1 m away from the fan. The microphone's stand was seated on a small table which was draped with sound absorbing material to minimize acoustic reflection. The microphone was calibrated using a B&K type 4220 pistonphone which generates a 250 Hz tone having an amplitude of 124 dB (re 20 $\mu$Pa). The unsteady rotor force was measured using a force sensor which was preloaded and positioned between the

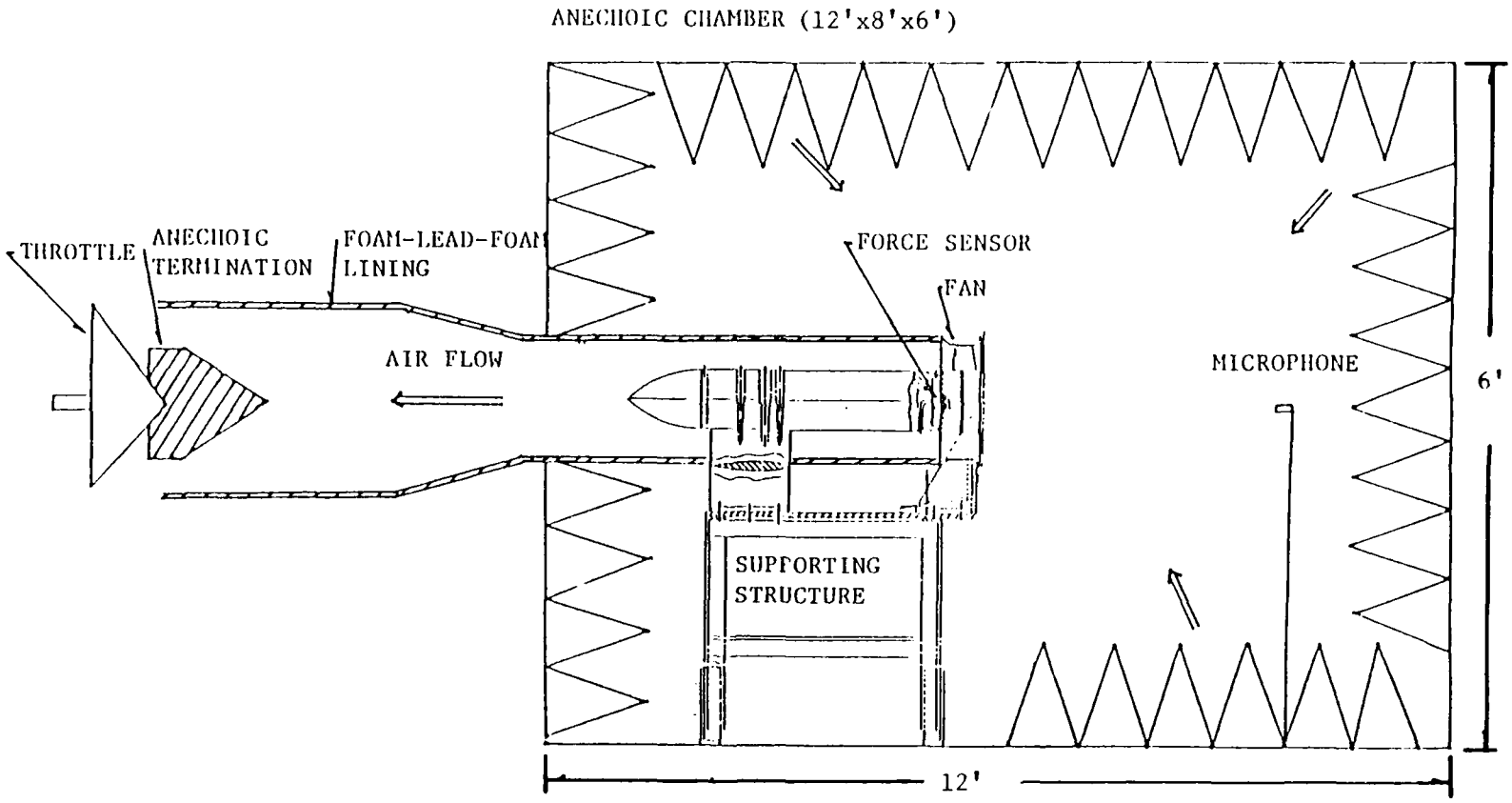


Figure 2.1 Experimental Setup for the Measurement of Unsteady Rotor Force and Fan Noise.

rotor and the root of the shaft as shown in Figure 2.2. Figure 2.3 shows the flow schematic for the measuring system.

## 2.3 Design and Calibration of the Measuring Device for Unsteady Rotor Force

### 2.3.1 The Design of the Force Sensor

The force sensor is a ring type, two-layer piezoceramic transducer as shown in Figure 2.4. It utilizes a piezoceramic as the sensing elements. The piezoceramic generates an electrical signal due to the dynamic deformation caused by the unsteady rotor force.

The force sensor was preloaded and positioned between the rotor and the root of the shaft as shown in Figure 2.2. In order to reduce the response of the transducer to the magnetic field force inside the fan motor, a low impedance transducer is desired. The impedance of a transducer is proportional to its thickness and to the inverse of the dielectric constant of the piezoceramic used [20]. A high dielectric constant will reduce the impedance, as will a small thickness. On the other hand, the sensitivity of the transducer is proportional to the thickness of the piezoceramic elements. In order to obtain a high sensitivity, low impedance transducer, a two-layer piezoceramic element was used. A two-layer transducer possesses lower impedance than a one-layer transducer of the same total thickness. A piezoceramic with a high dielectric constant (K=3200) was selected. A shielding device, as

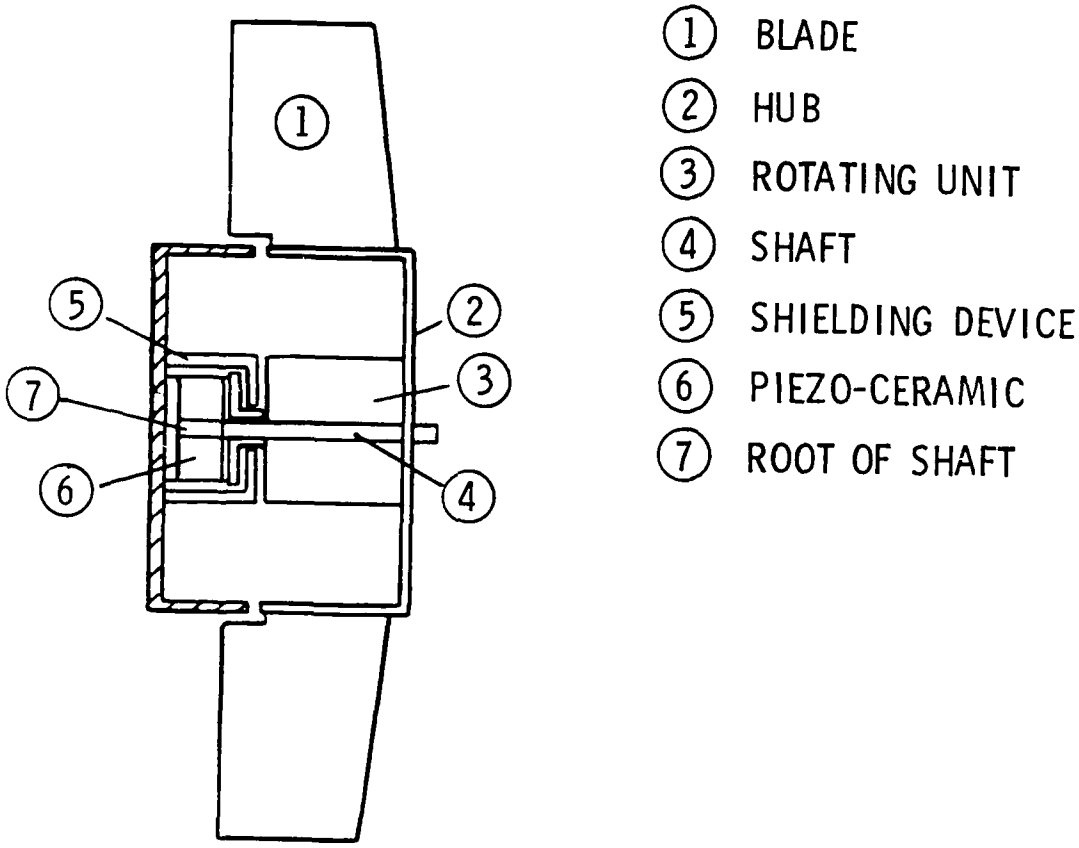


Figure 2.2 Measuring Device for Unsteady Rotor Force.

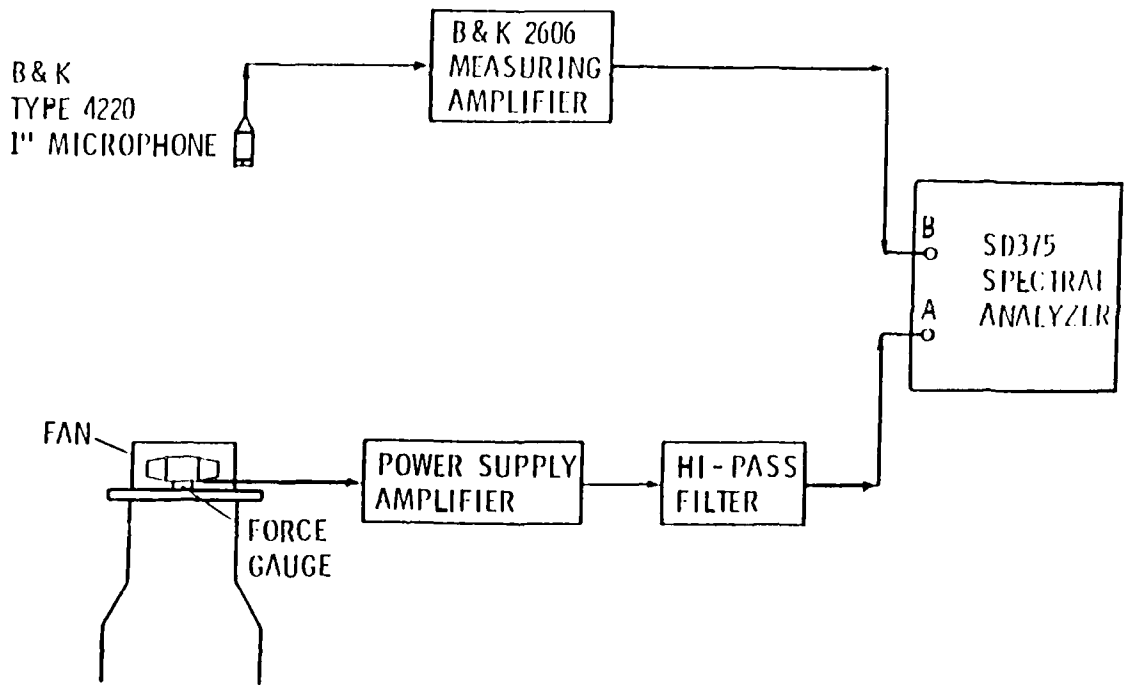


Figure 2.3 Flow Schematic for the Measuring System.

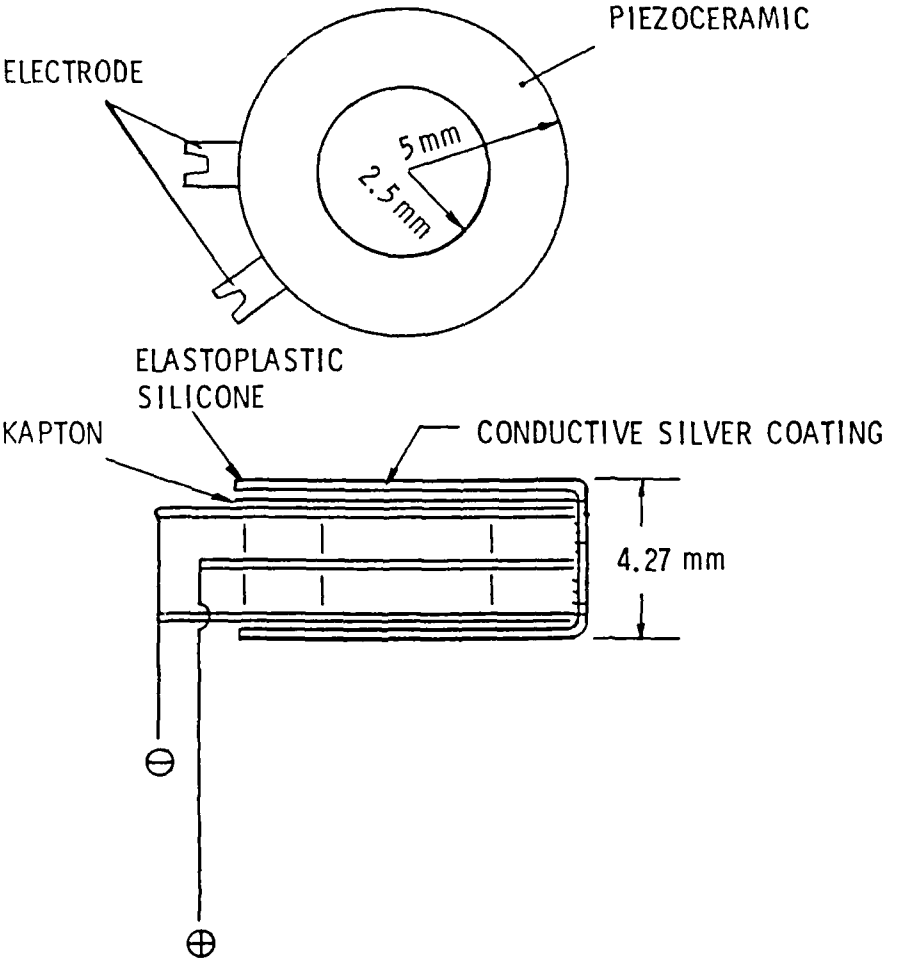


Figure 2.4 Construction of the Force Sensor.

shown in Figure 2.2, and a conductive silver coating were used to shield the transducer from the magnetic field.

### 2.3.2 Calibration of the Unsteady Rotor Force Measuring System

Figure 2.5 shows the experimental setup for the dynamic calibration of the measuring system. Firstly, the fan rotor was removed and an impact force was applied to the force sensor. Figure 2.6(a) shows the shock spectrum from the force sensor. Since an impact force and random noise in the frequency domain are equivalent, the shock spectrum corresponds to the frequency response of the measuring system. It shows that the frequency response of the measuring system with the rotor removed is flat up to 1600 Hz. A sinusoidal unsteady axial force with swept frequency was then applied to the system (with the rotor installed with and without blades). The frequency responses of the system are shown in Figure 2.6(b) and (c). This result indicates significant coupling between the force sensor and rotor. The 600 Hz peak shown in Figure 2.6(c) is due to a resonance of the blades. The transfer functions at the BPF and its harmonics were obtained from Figure 2.6(c). The coherence functions associated with both transfer functions in Figure 2.6(b) and (c) are nearly unity over the testing frequency range.

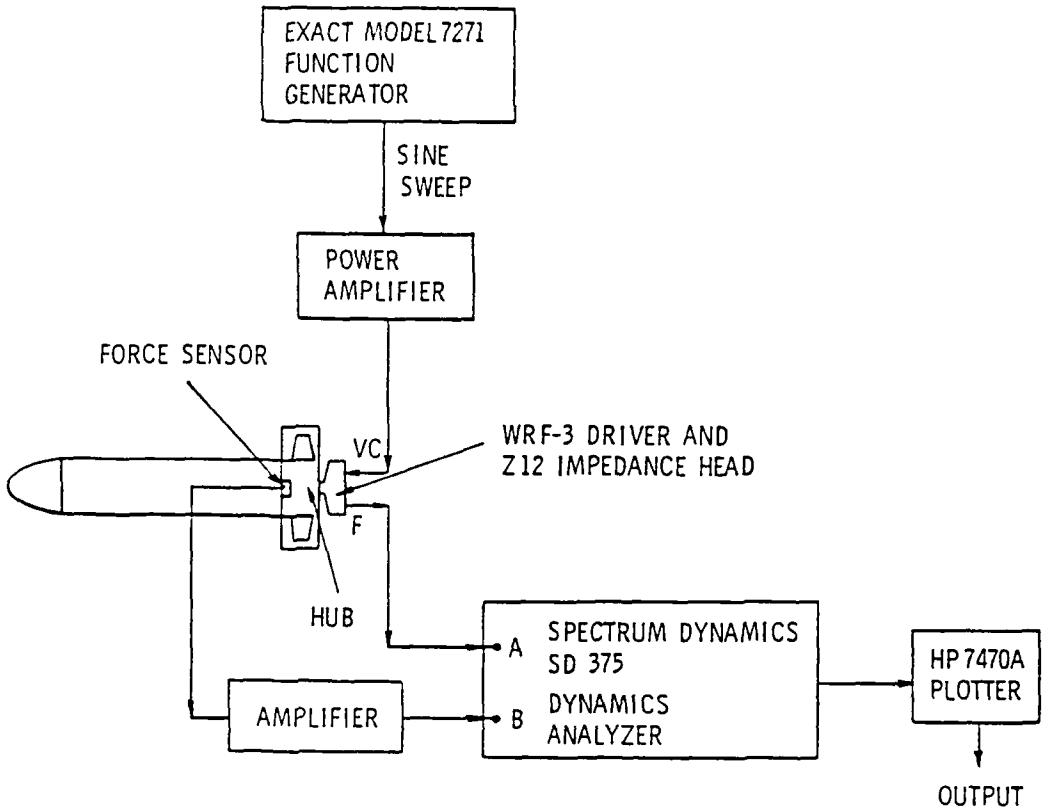


Figure 2.5 Experimental Setup for the Calibration of Rotor Force Measuring Device.

(a)

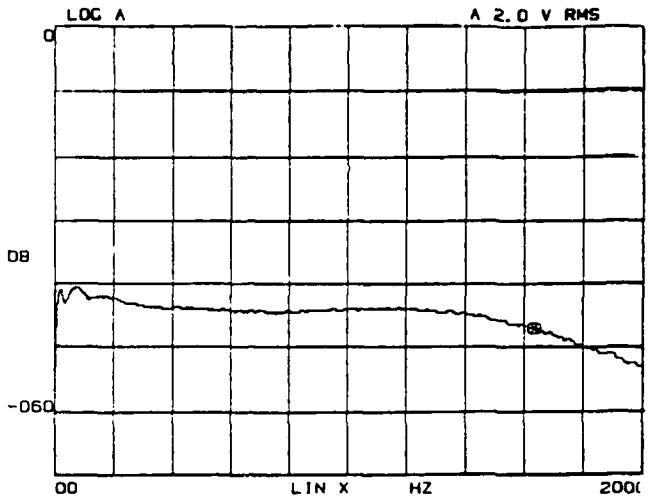


(b)

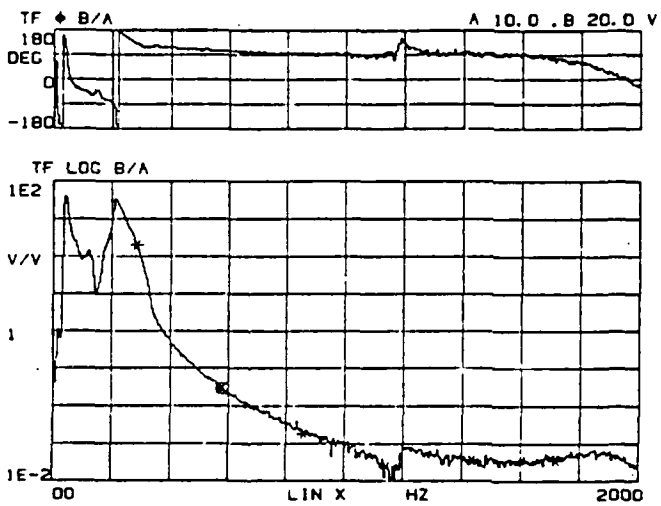


Figure 2.6 Frequency Response of Rotor Force Measuring Device
(a) Transducer Only
(b) Transducer and Rotor Without Blades
(c) Transducer and Rotor

(c)

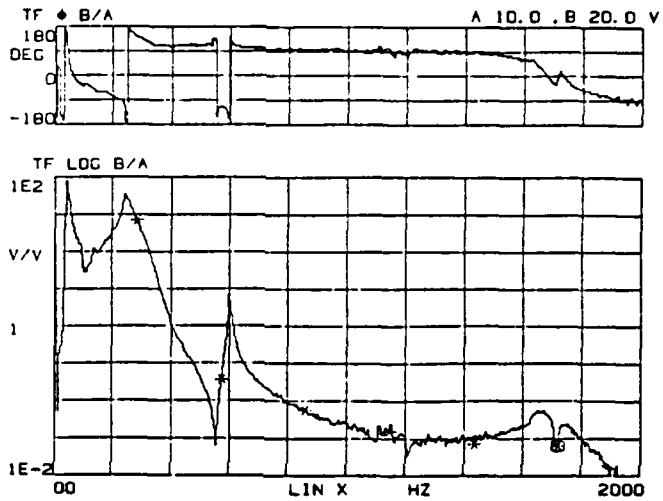


Figure 2.6 (continued)

## 2.4 Experimental Results and Discussions

The coherent output power spectrum and the coherence function for the unsteady rotor force and fan noise were used to indicate the contribution of unsteady loading to the fan noise. Figure 2.7 shows typical experimental data for the case without any obstruction in front of the fan. The coherent output power spectrum and the total output power spectrum are very close together at the BPF. This shows that the noise at the BPF is dominated by the unsteady loading and not the steady loading. The slope in the phase diagram is indicative of the time delay for the sound propagation from the fan to the microphone. This phase response verifies that the measured noise is indeed correlated to the unsteady loading. The fluctuating phase distribution at higher frequencies, greater than 1.1 kHz, suggests that the fan is no longer a compact source at those frequencies. The fluctuating phase distribution at frequencies below the BPF is due to the acoustic limitation of the anechoic chamber. The dip in the frequency range between 500 Hz and 580 Hz is due to coupling between the force sensor and fan structure.

For the case of a cylinder in front of the center of the fan, the cylinder is expected to generate a two-cycle distortion which should enhance the unsteady blade loading. Figure 2.8 shows that the coherent output power spectrum and the total output power spectrum are in close agreement not only at the BPF, but at the first and the third harmonic also. These harmonics are enhanced by the two-cycle inflow distortions

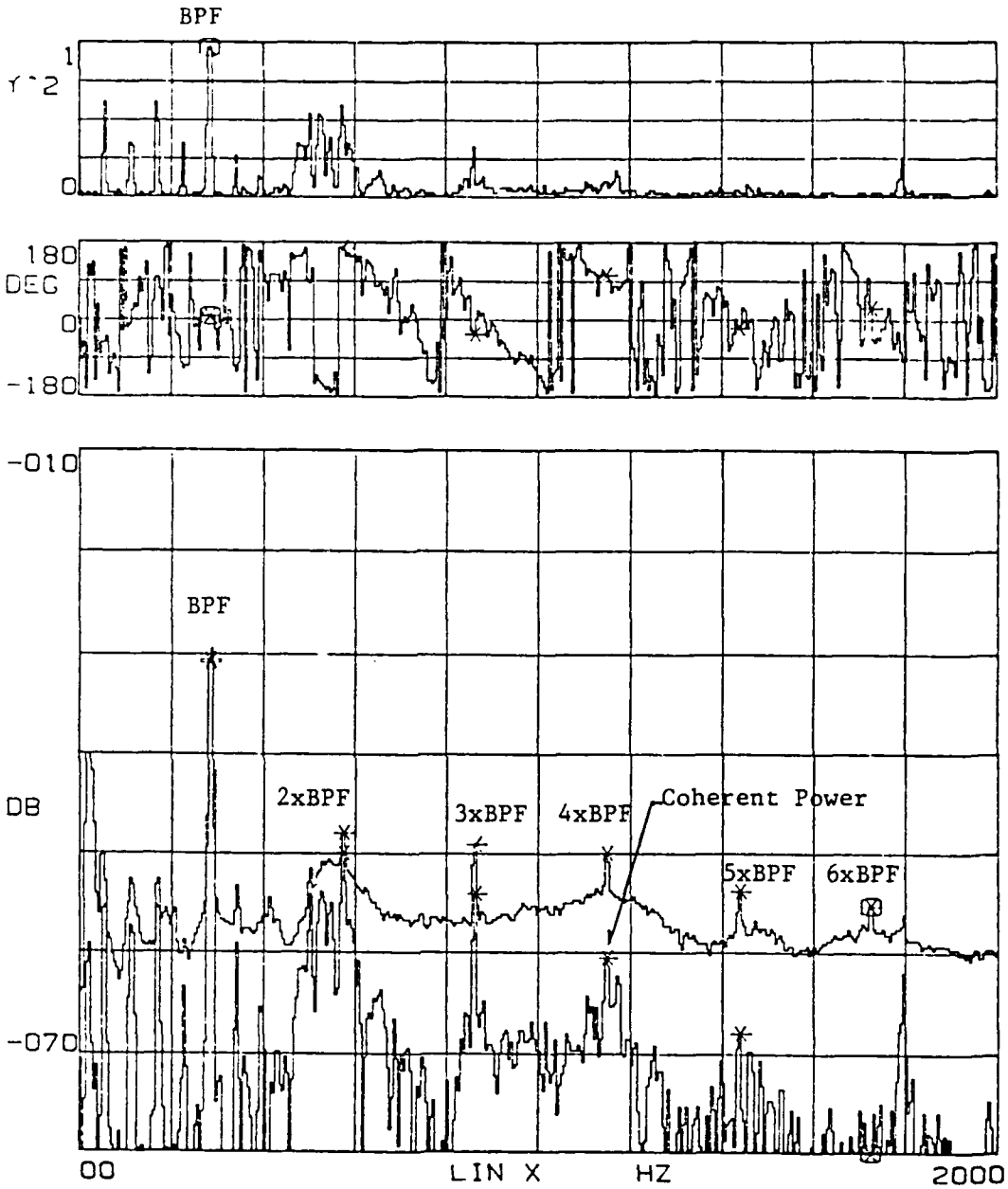


Figure 2.7 Comparison of Sound Power Spectrum and Coherent Power Spectrum of a Patriot Fan.

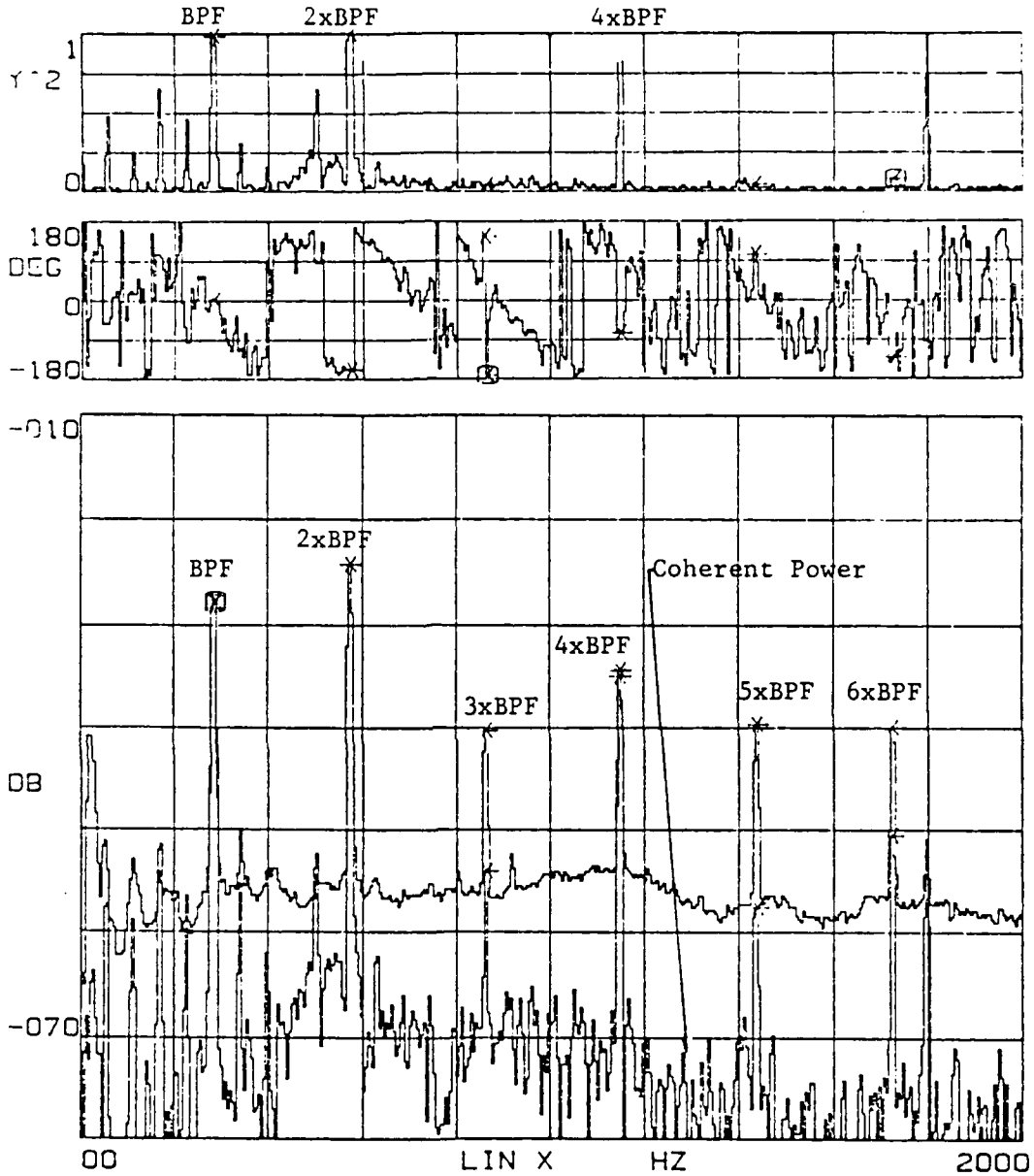


Figure 2.8 Comparison of Sound Power Spectrum and Coherent Power Spectrum of a Cylindrical Obstructed Patriot Fan.

created by the cylinder. Again, the slope in the phase diagram verifies that the measured noise is due to the unsteady rotor loading.

These results support the theory that discrete-frequency noise at the BPF and its harmonics is dominated by unsteady rotor loading. For the test fan, the unsteady loading at the BPF is apparently due to an interaction between the fan outflow and a strut situated downstream and close to the blades. This hypothesis was not verified quantitatively. The unsteady loading at the harmonics of the BPF results from the interaction of the blades and the distorted inflow. Figure 2.8 verifies this conclusion. The data also show that the broadband noise is weakly correlated to the measured unsteady rotor loading.

# Chapter 3

# MEASUREMENT OF TIME INVARIANT SPATIAL INFLOW VELOCITY AND COMPUTATION OF DISCRETE-TONE SOUND RADIATION

## 3.1 Introduction

The principal source of discrete-frequency noise is caused by the interaction of the blades with the circumferentially distorted inflow. The circumferentially distorted inflow velocity can be Fourier decomposed into a sum of sinusoidally varying components with various amplitudes and frequencies. As the blades pass through such a sinusoidally varying velocity field, a sinusoidal variation in blade loading will occur. This causes the blades to radiate sound as dipole sources.

A 1.27 cm diameter cylindrical obstruction was positioned at several different radial locations where Washburn [18] found that significant discrete-frequency noise was generated. These locations are shown in Figure 3.1. The three-dimensional steady-state velocity field was measured using miniature five-hole probes [21]. The inflow velocity vectors were then decomposed into a circumferential average velocity and a circumferential non-uniform component using Fourier analysis. Based on the measured blade geometries, the unsteady rotor force was computed using an unpublished Computational Fluid Dynamics (CFD) package which was developed at the Pennsylvania State University

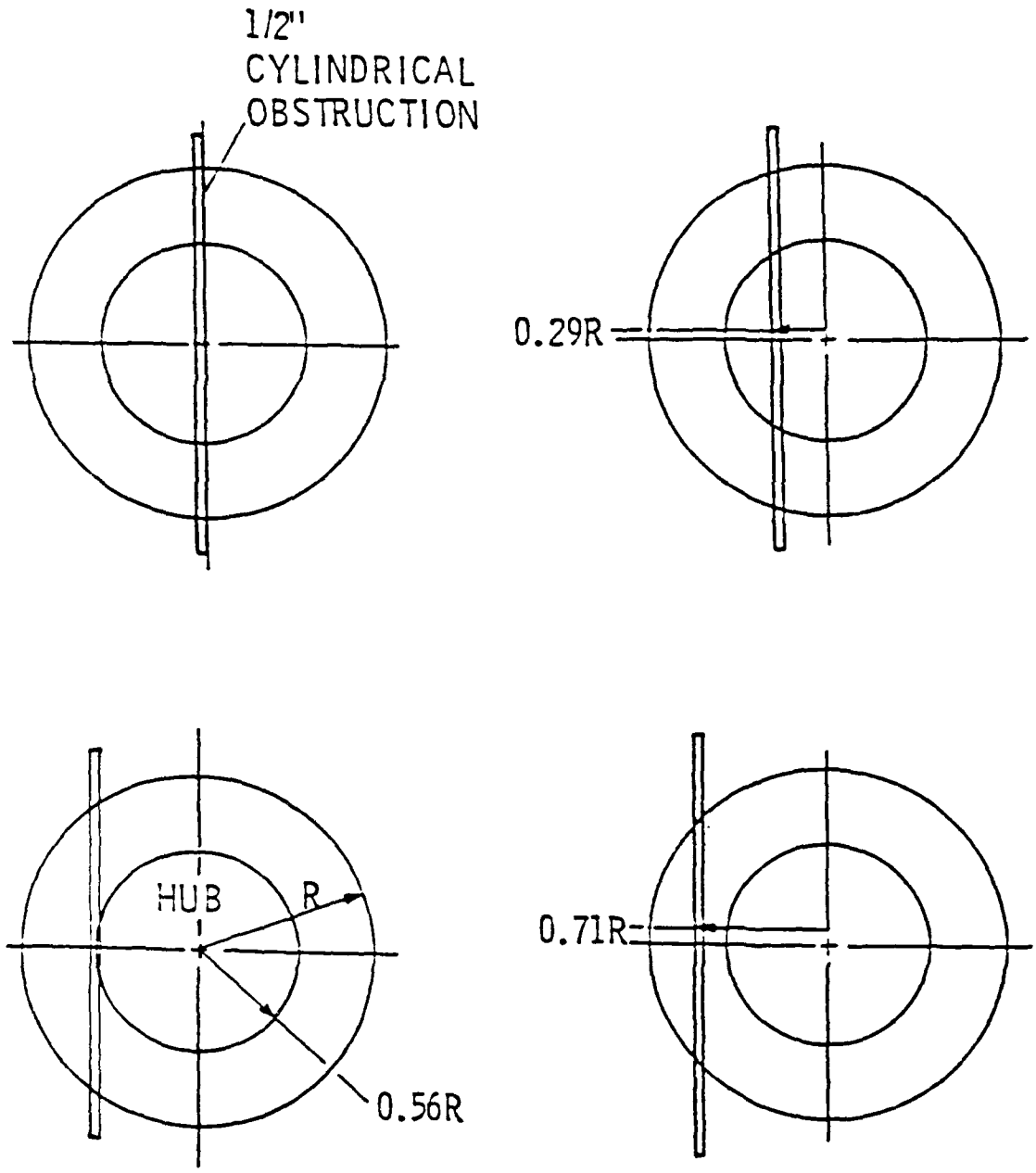


Figure 3.1 Radial Locations of a 1.27 cm Cylindrical Obstruction.

[22]. Then, the discrete-frequency noise was computed using a dipole source model. Figure 3.2 shows the steps in the computation of the discrete-frequency noise. The comparison between computational results and experimental results is presented in this chapter.

## 3.2 Experimental Determination of Spatial Velocity Distribution at the Inlet of a Rotating Fan

### 3.2.1 Experimental Setup

The experiments were conducted in the same anechoic chamber as described in section 2.2. Figure 3.3 shows the experimental apparatus. The circumferential variation of the inflow velocity was measured using three five-hole probes. These probes were spaced 120 degrees apart and mounted on a rotating unit which was driven by a stepping motor. The rotating unit consisted of a fan shroud and a dummy hub which were used to simulate the boundary condition of a Patriot fan. The flow field at the inlet of the rotating unit is thus similar to that of a Patriot fan. A running Patriot fan was used to ingest air into the rotating unit. The five-hole probe support struts were positioned parallel to the fan blade leading edge. The five-hole probe could move along the same spatial locations relative to the fan inlet as the blade leading edge in a real fan. The concept is shown schematically in Figure 3.4. Figure 3.5 shows a photograph of the device assembly. The five-hole probes were positioned at a total of nine different fan radii to measure the circumferential velocity distributions. The rotating unit

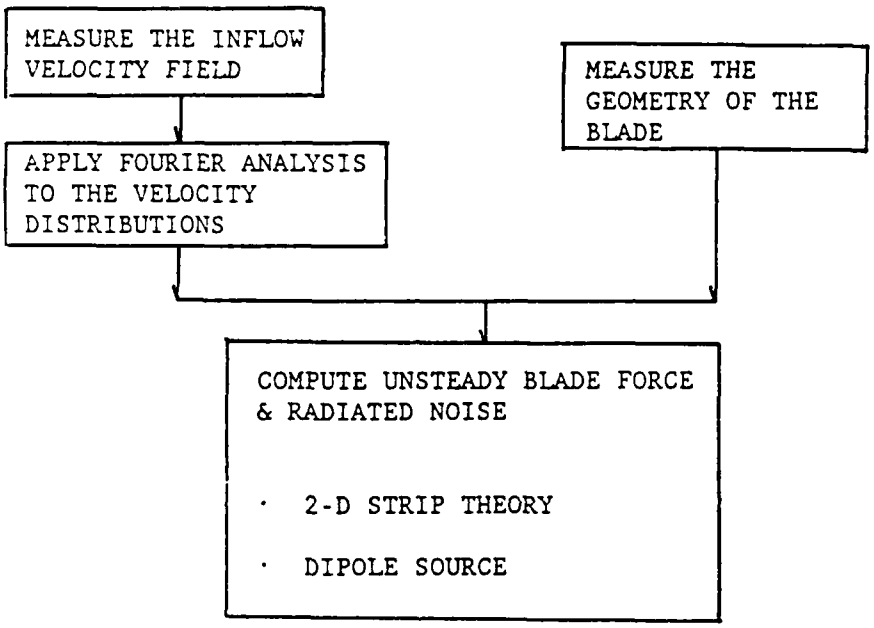


Figure 3.2. The Flow Schematic for Calculating Unsteady Rotor Force and Radiated Noise.

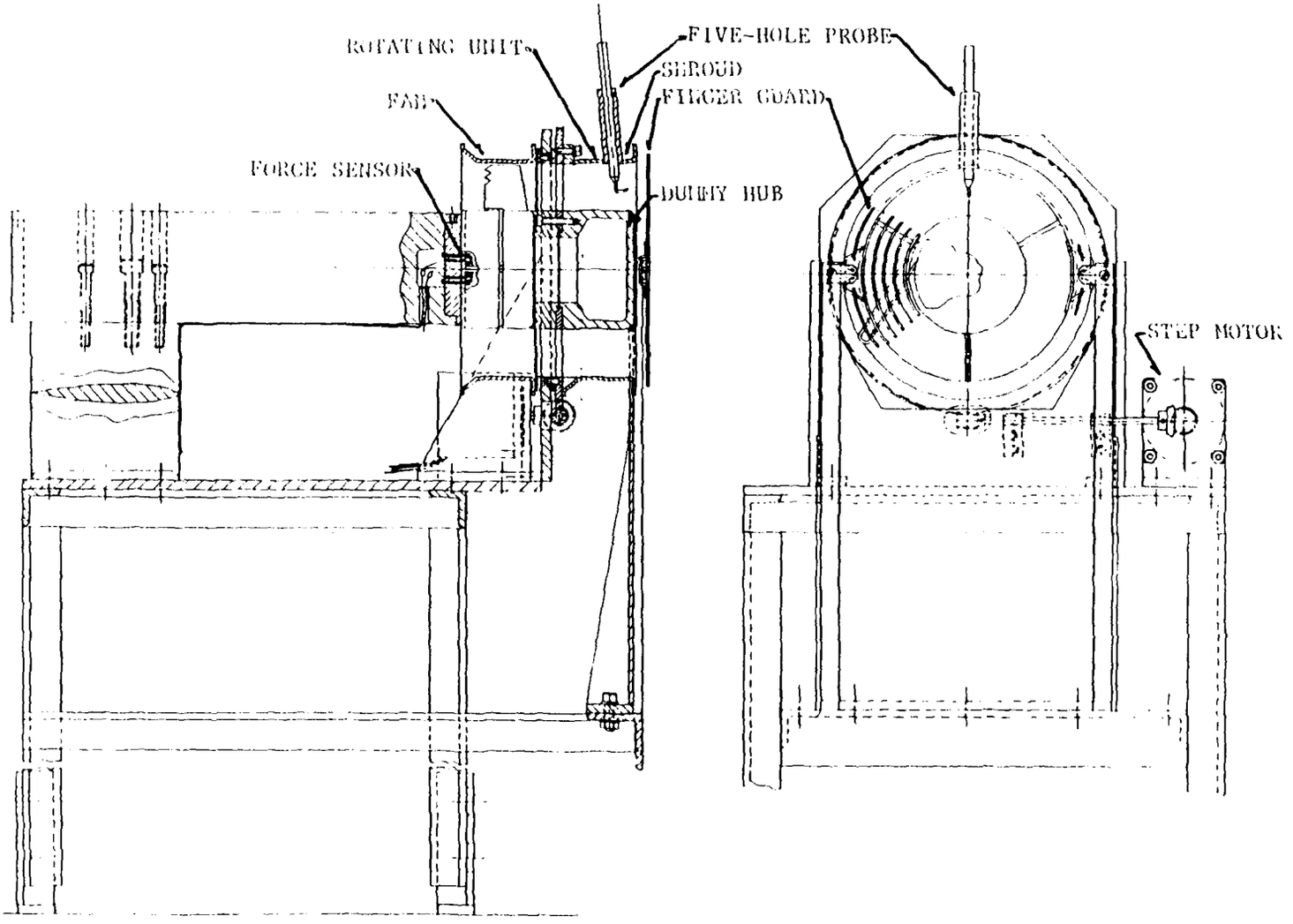


Figure 3.3 Experimental Device Assembly.

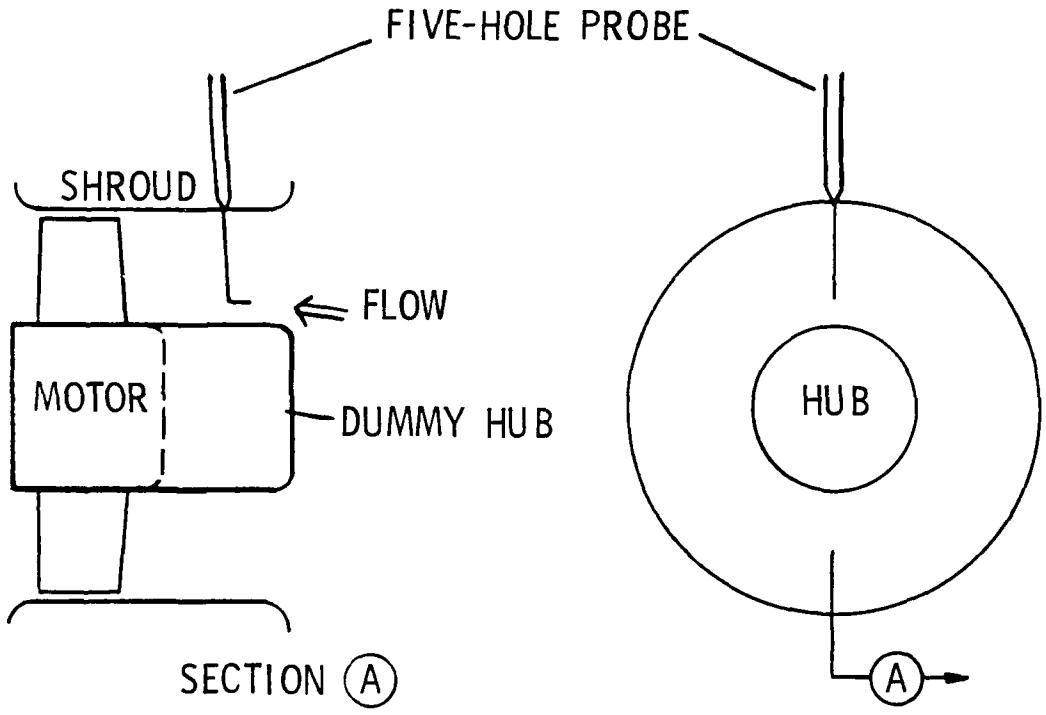


Figure 3.4 General Concept for Inflow Velocity Measurement.

Side View

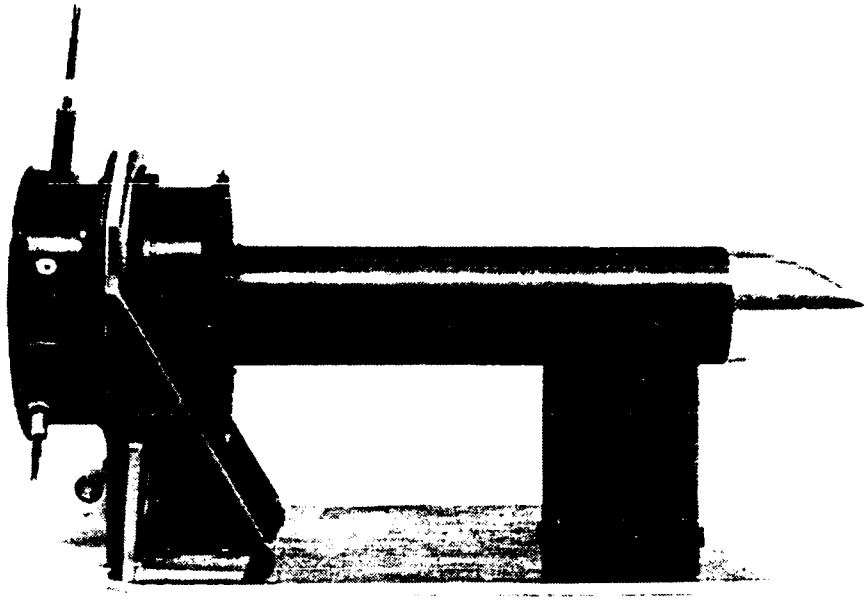

Front View

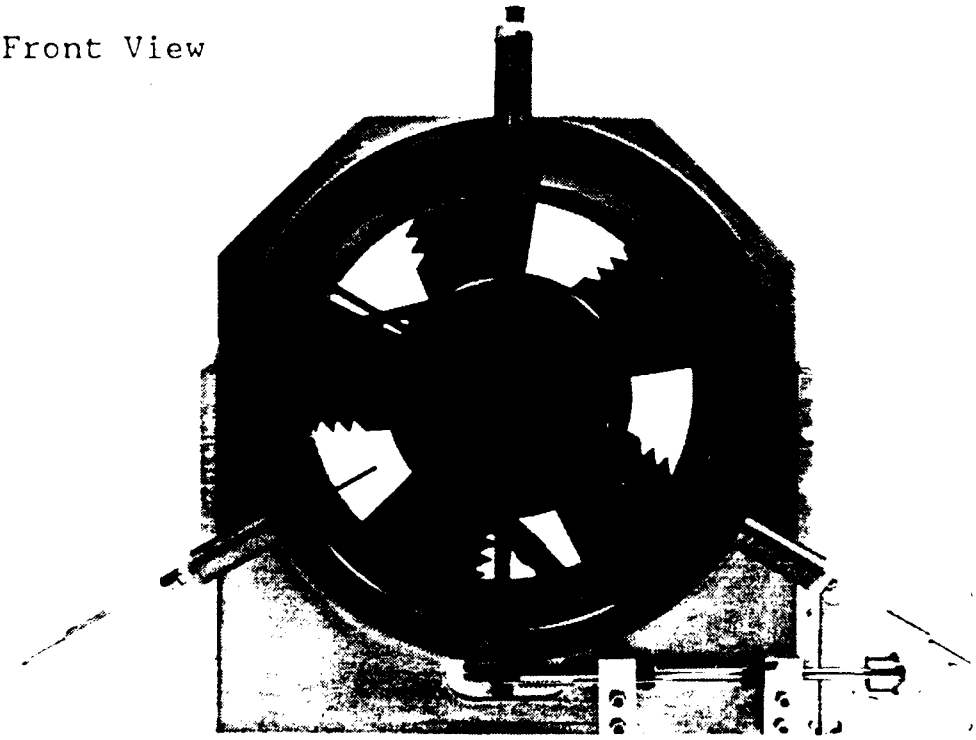

Figure 3.5 Photograph of the Experimental Device Assembly.

traverses the probes through 360° in 3° increments. A sampling number of 120 data points per revolution was used to prevent aliasing in the Fourier coefficient estimates which will be explained in section 3.3.1.

### 3.2.2 Five-Hole Probe

A five-hole probe was used to measure the inflow velocity because of the following considerations:

1. The flow passing through the blades is three-dimensional; therefore, the velocity transducer should be able to discriminate flow direction.
2. The inflow velocity field is, under practical application considered stationary. Since only time-averaged flow velocity is required, a transducer with a slow response can be utilized.

Figure 3.6 shows the basic configuration of an angle-tube type probe. The flow angle and velocity can be computed from the pressure sensed at each of the five holes. The pressure sensed by the probe can be related to the flow angle and velocity using calibration data.

The probes were calibrated for an air flow speed range between 6 m/sec and 21 m/sec. A schematic diagram of the calibration setup is shown in Figure 3.7. The calibration process consists of placing the probe in a known flow field which was supplied by an open jet as shown in Figure 3.7. The calibration curves consist of measured pressures

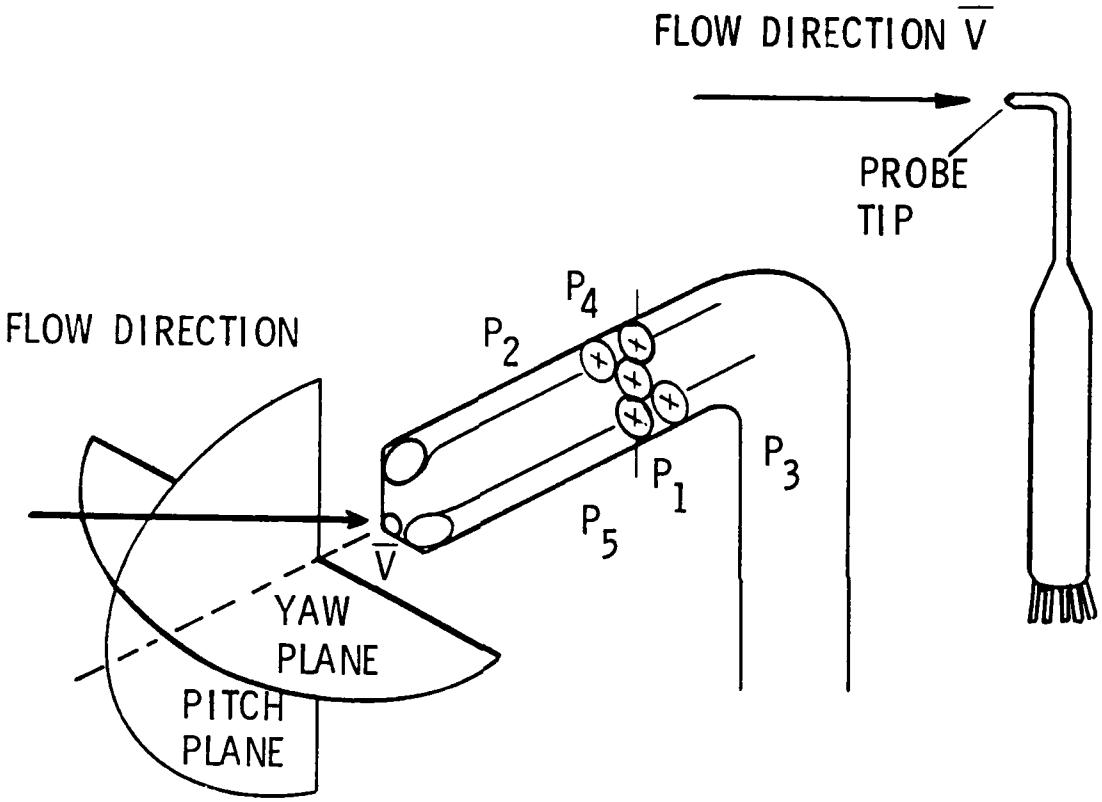


Figure 3.6 Geometry of the Angle-Tube Probes.

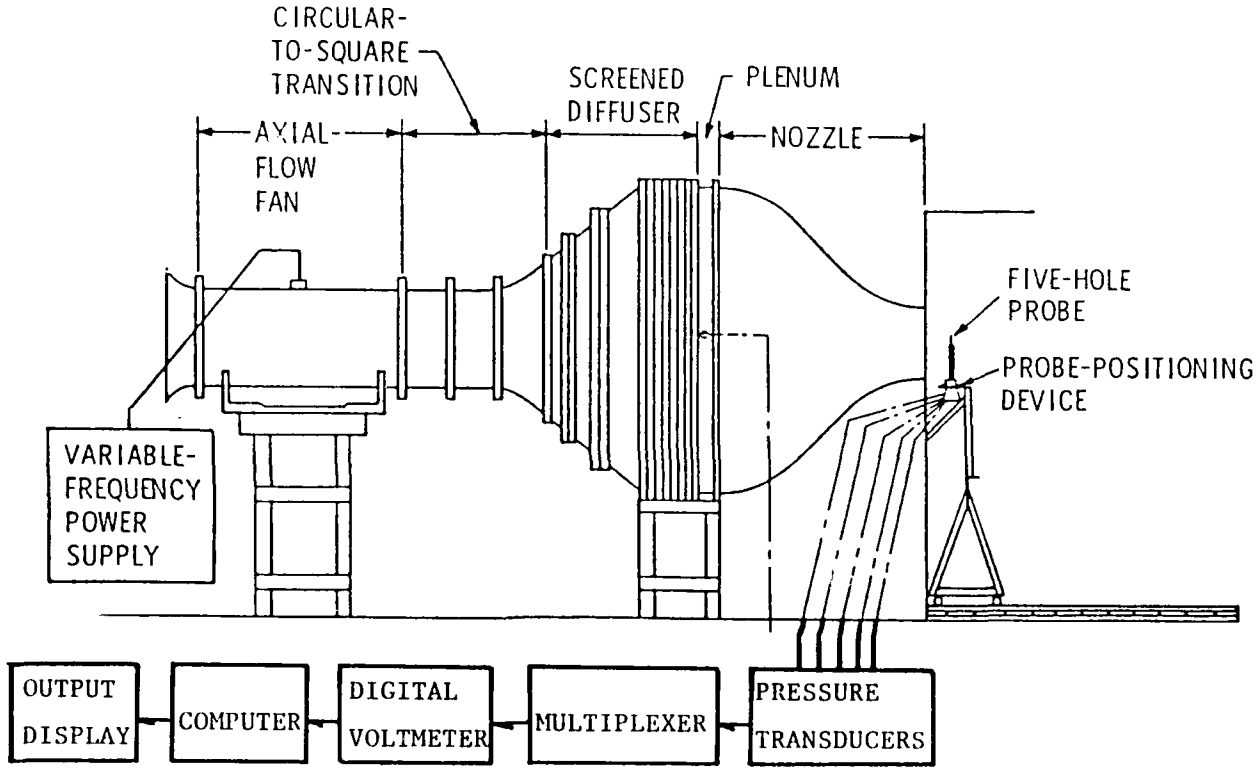


Figure 3.7 Calibration Schematic (open-jet facility).

versus air velocity, yaw angle, and pitch angle of the probe. These families of curves are coupled with equations of the Bernoulli type to form unique relationships between the various variables. The procedure is well documented by Treaster and Yocum [21] and is not repeated here. Figure 3.8 shows a schematic diagram of the five-hole probe measuring system. The signal which corresponds to the pressures at each of the five holes were scanned by a multiplexer and processed on a Vax 11/780 computer. Based on the pre-established calibration data, the inflow velocity and direction were estimated. The accuracy of the resulting data is estimated to be $\pm$ 1%.

### 3.2.3 Experimental Results

Experimental results for a fan with no obstruction and with a 1.27 cm diameter cylinder in front of the fan are presented. The circumferential distribution of axial, tangential, and radial velocities in the blade leading edge plane was measured. Figure 3.9 shows the definitions of the axial, tangential, and radial velocity components. Because of the large database, only a few selected typical results are presented.

Figure 3.10 shows the circumferential velocity distribution at one fan radius over the 360$^{o}$ sector for the cases of the fan operating with and without a cylinder in front of the center of the fan. The abscissa represents the circumferential location of the probe relative to the initial position which is the bottom of the fan. The ordinate represents the normalized local mean velocity which is equal to the

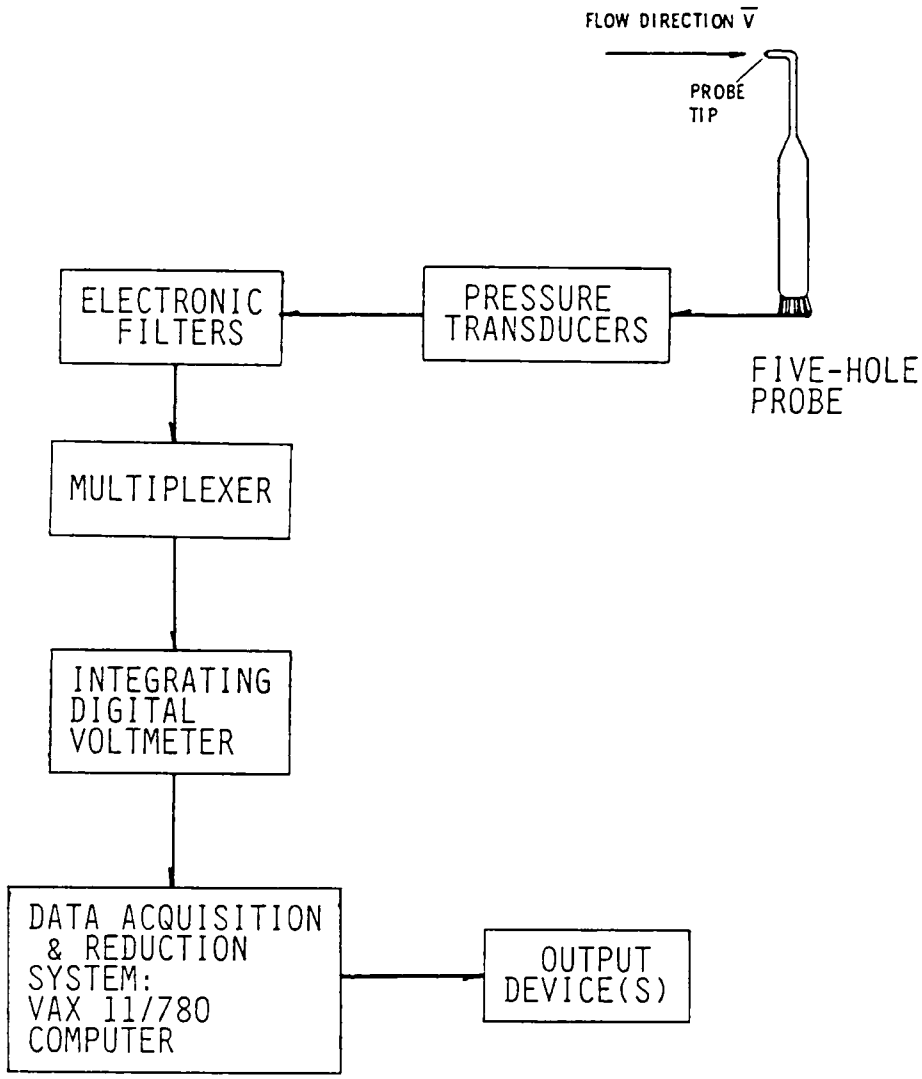


Figure 3.8 Schematic Diagram of the Five-Hole Probe System.

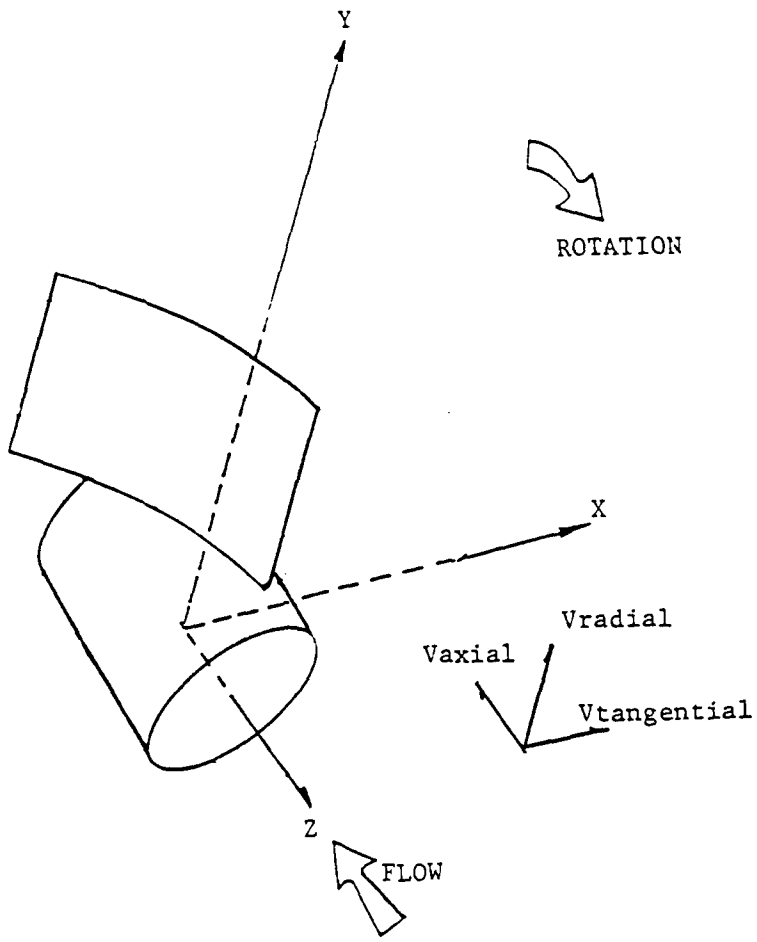


Figure 3.9 Coordinate System for the Inflow Velocity

(a)

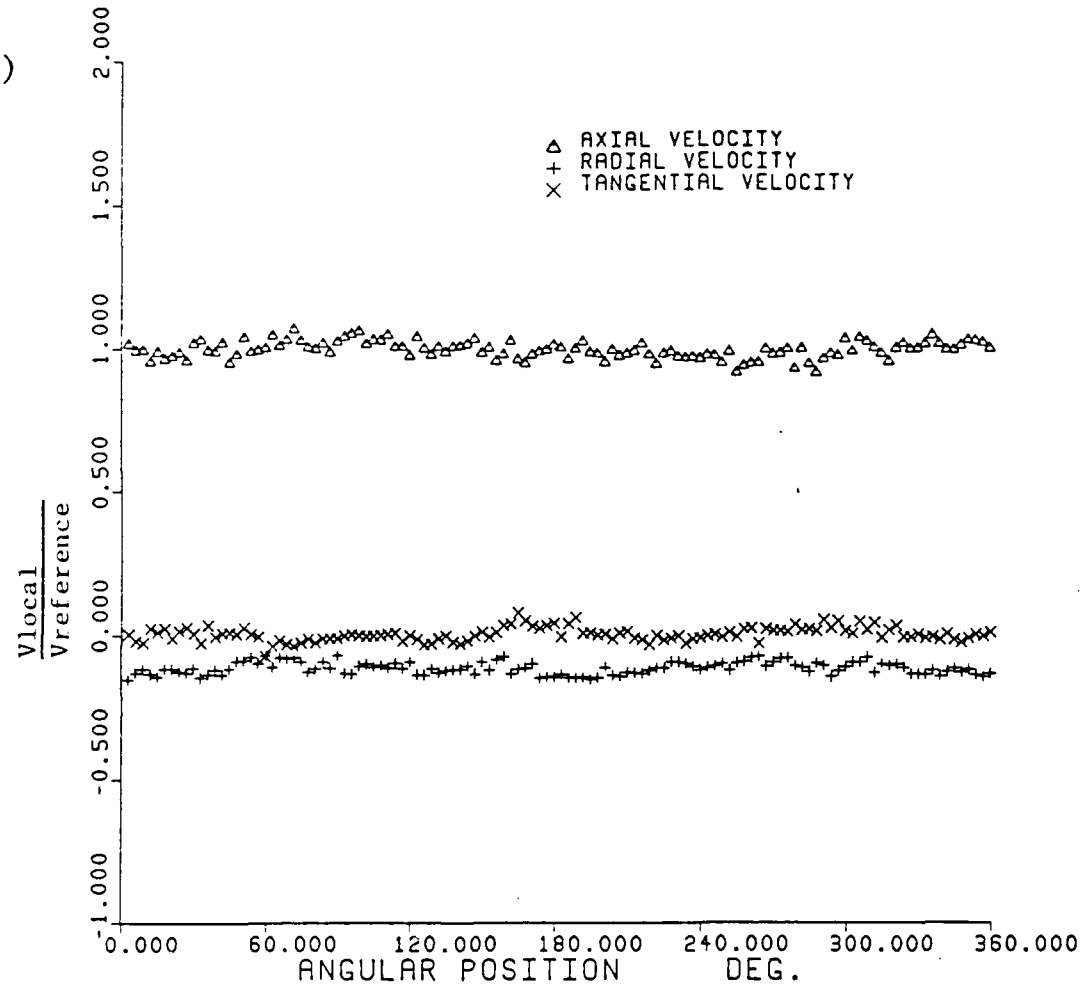


Figure 3.10 Typical Dimensionless Circumferential Velocity Distributions.
(a) A Fan Without Obstruction
(b) A Fan With a Cylinder in Front of the Center of the Fan

(b)

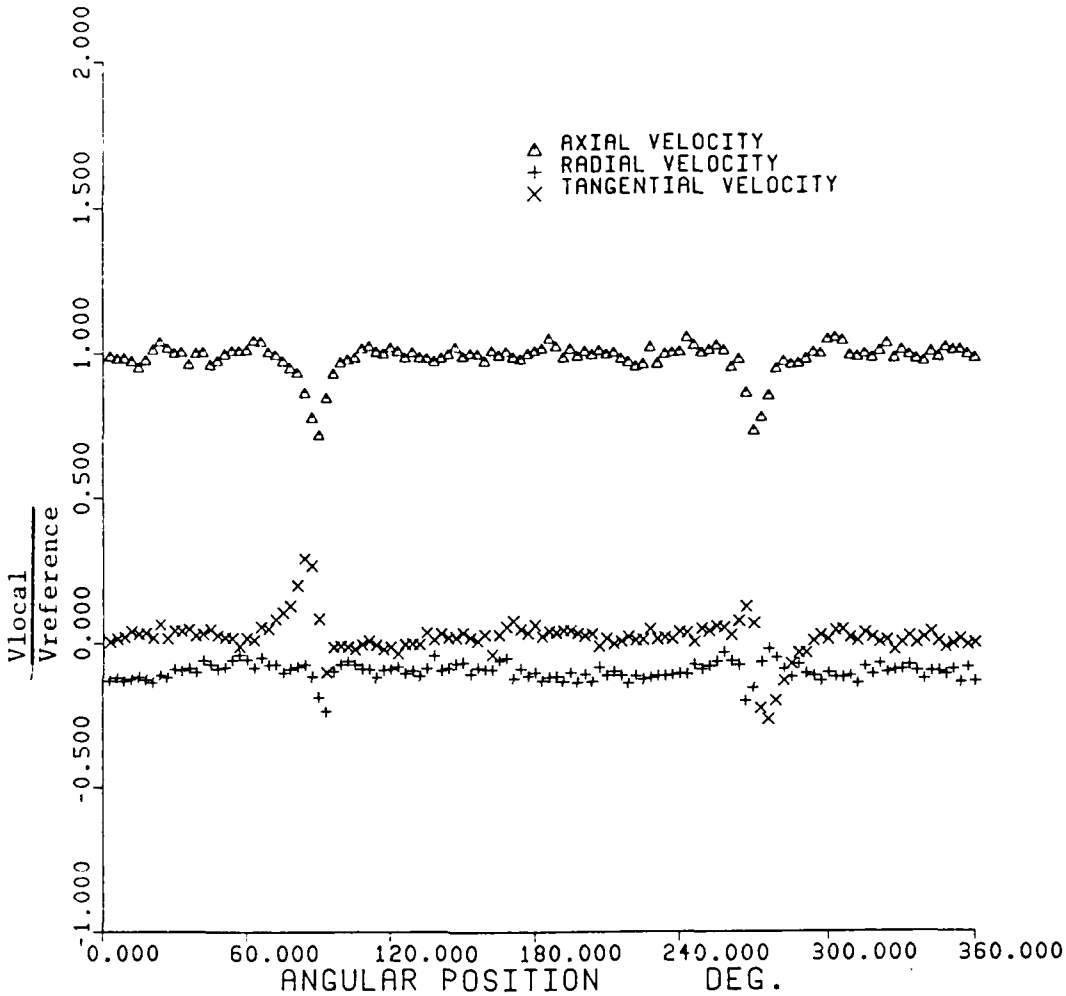


Figure 3.10 (continued)

local mean velocity divided by a reference velocity, measured in the exhaust duct. The reference velocity is 8.7 m/sec. The velocity distributions for the case without a cylinder are quite uniform as shown in Figure 3.10 (a). For the case of a cylinder in front of the center of the fan, the pronounced variations in the data are a consequence of the cylinder wake. The variation of the tangential component of the inflow is due to potential flow around the cylinder.

Figure 3.11 shows the normalized axial component of mean velocity distribution in the plane of the blade leading edge. There was no cylinder in front of the fan. It shows that the maximum axial inflow velocity occurs at the region near the fan shroud. Figure 3.12 shows the secondary inflow distribution for the cases without a cylinder and with a cylinder placed at the various positions noted in Fig. 3.1. The secondary velocity was obtained by subtracting the mean axial velocity from the local inflow velocity. The arrows represent vectors showing the direction and the magnitude of the dimensionless, local secondary velocity. The rotational flow is caused by vorticity in the wake of the cylinder. It also shows that the secondary velocity increases and rotates in the direction coincident with the direction of the rotating blades as the flow approaches the region near the hub. Figure 3.13 shows polar plots of the circumferential distribution of axial velocity behind a cylinder at various radii. The dips in the plots indicate the axial component of the velocity defect caused by the cylinder wake. The maximum wake width occurs around 0.7 radius. The wake width decays in the regions close to the shroud and hub due to three-dimensional and

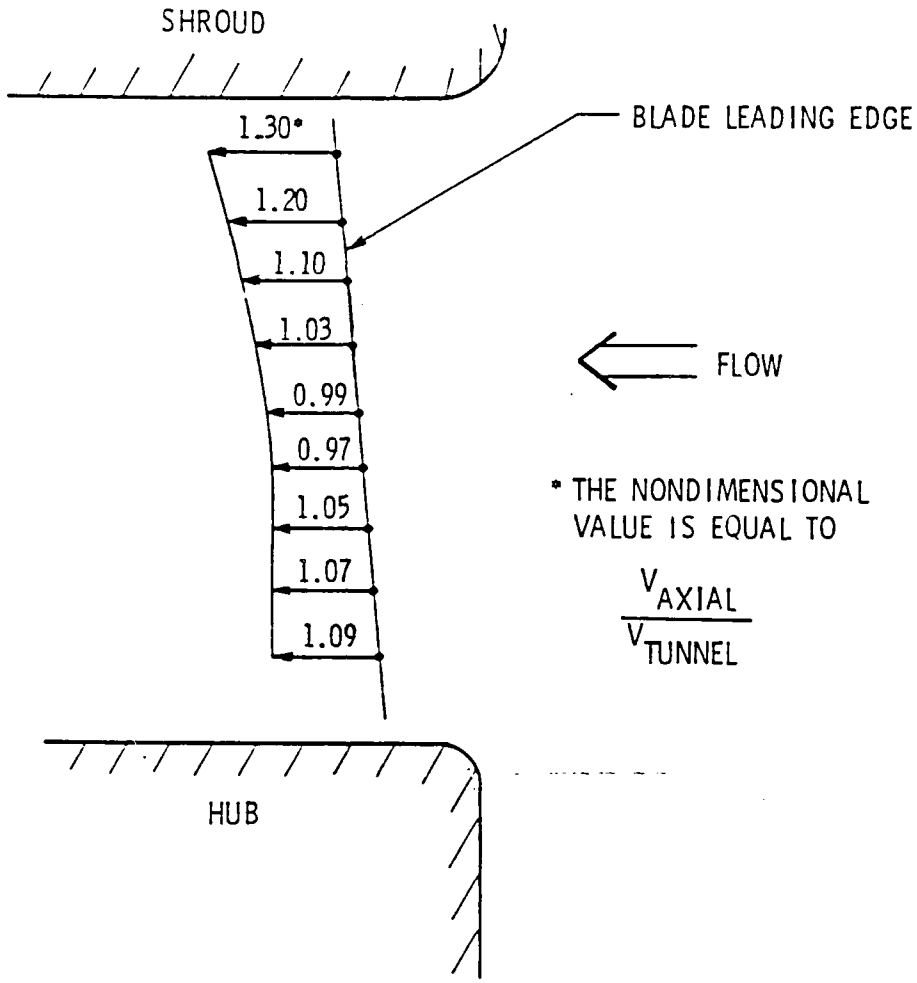


Figure 3.11 The Profile of Axial Velocity in the Plane of Blade Leading Edge.

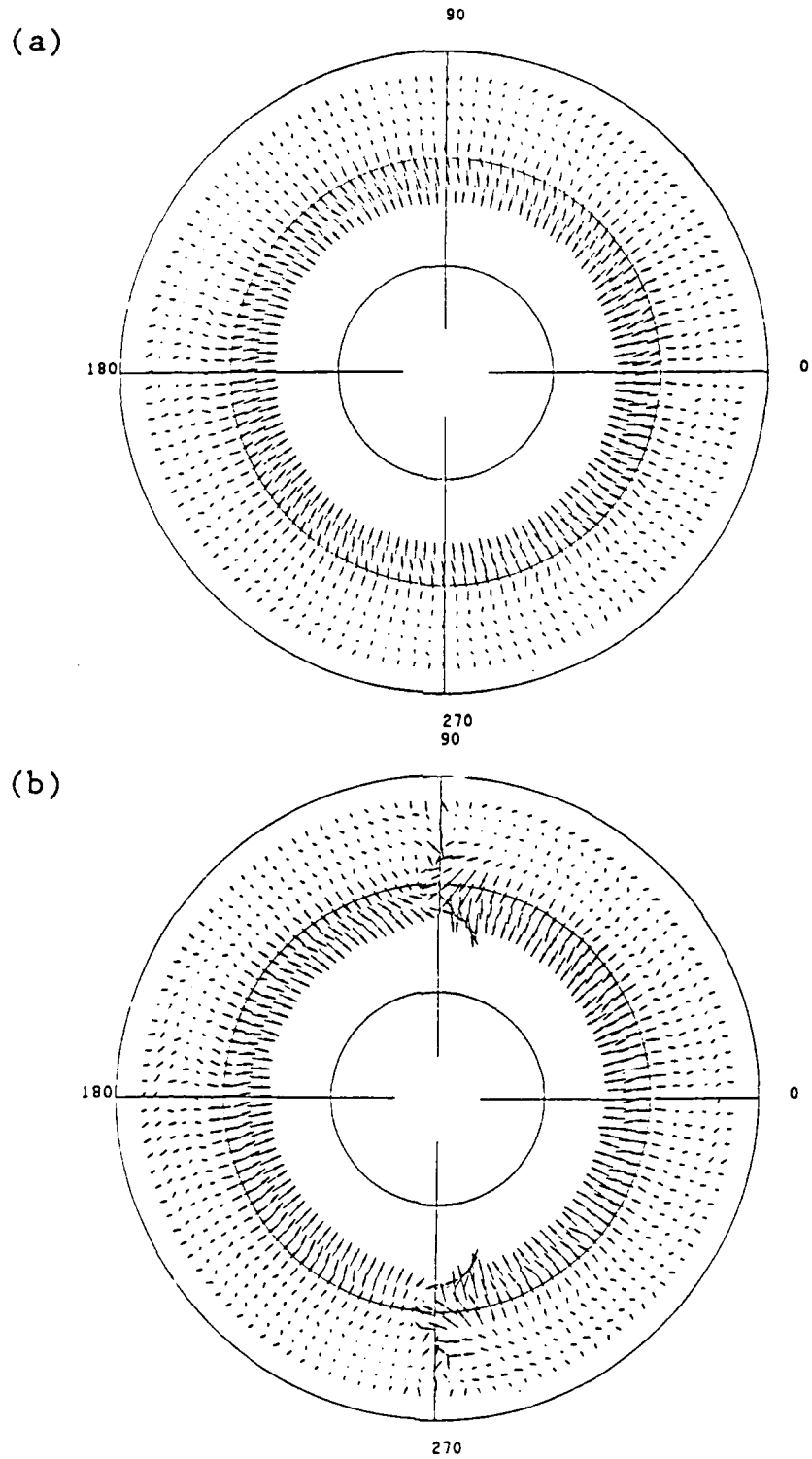


Figure 3.12 Secondary Flow as Measured in the blade plane of a Patriot fan
(a) Without Obstruction
(b) Cylinder at 0.0R
(c) Cylinder at 0.28R
(d) Cylinder at 0.50R
(e) Cylinder at 0.71R

(c)

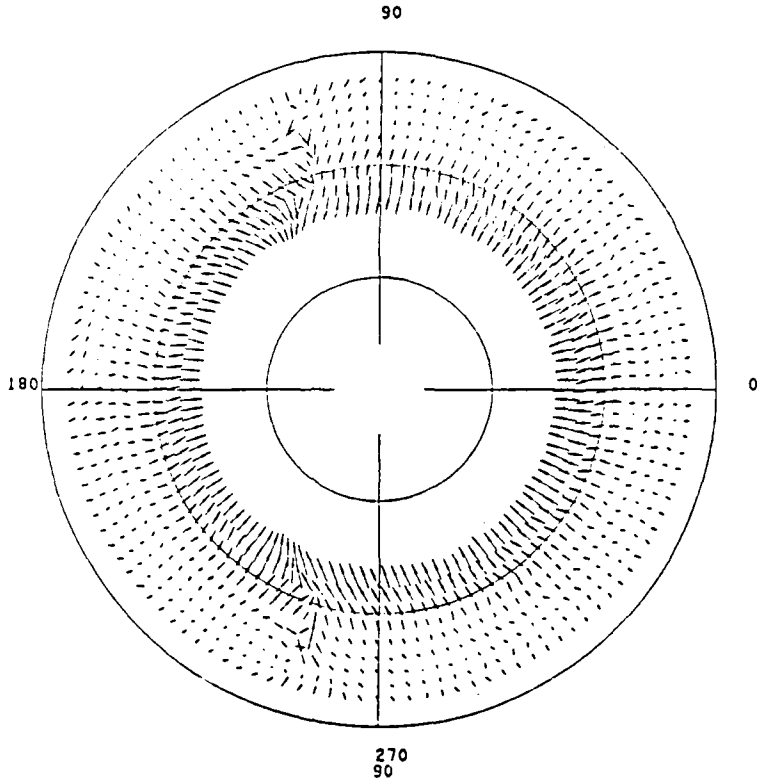


(d)

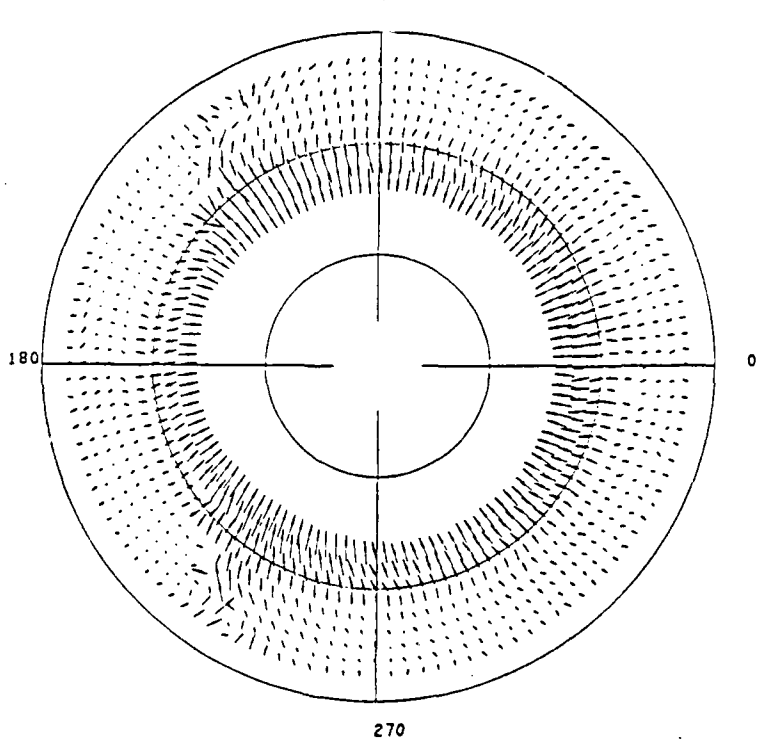


Figure 3.12 (continued)

(e)

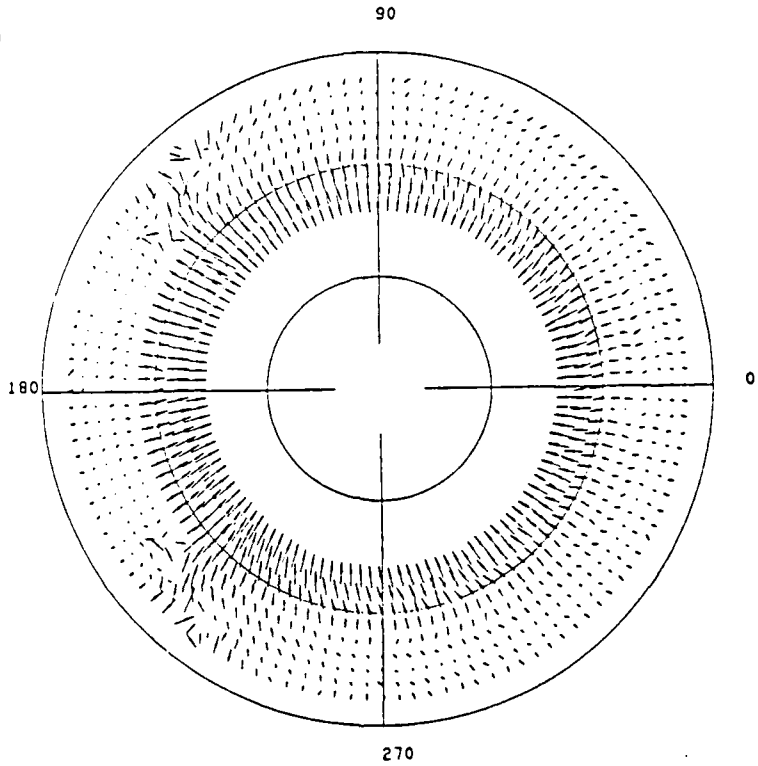


Figure 3.12 (continued)

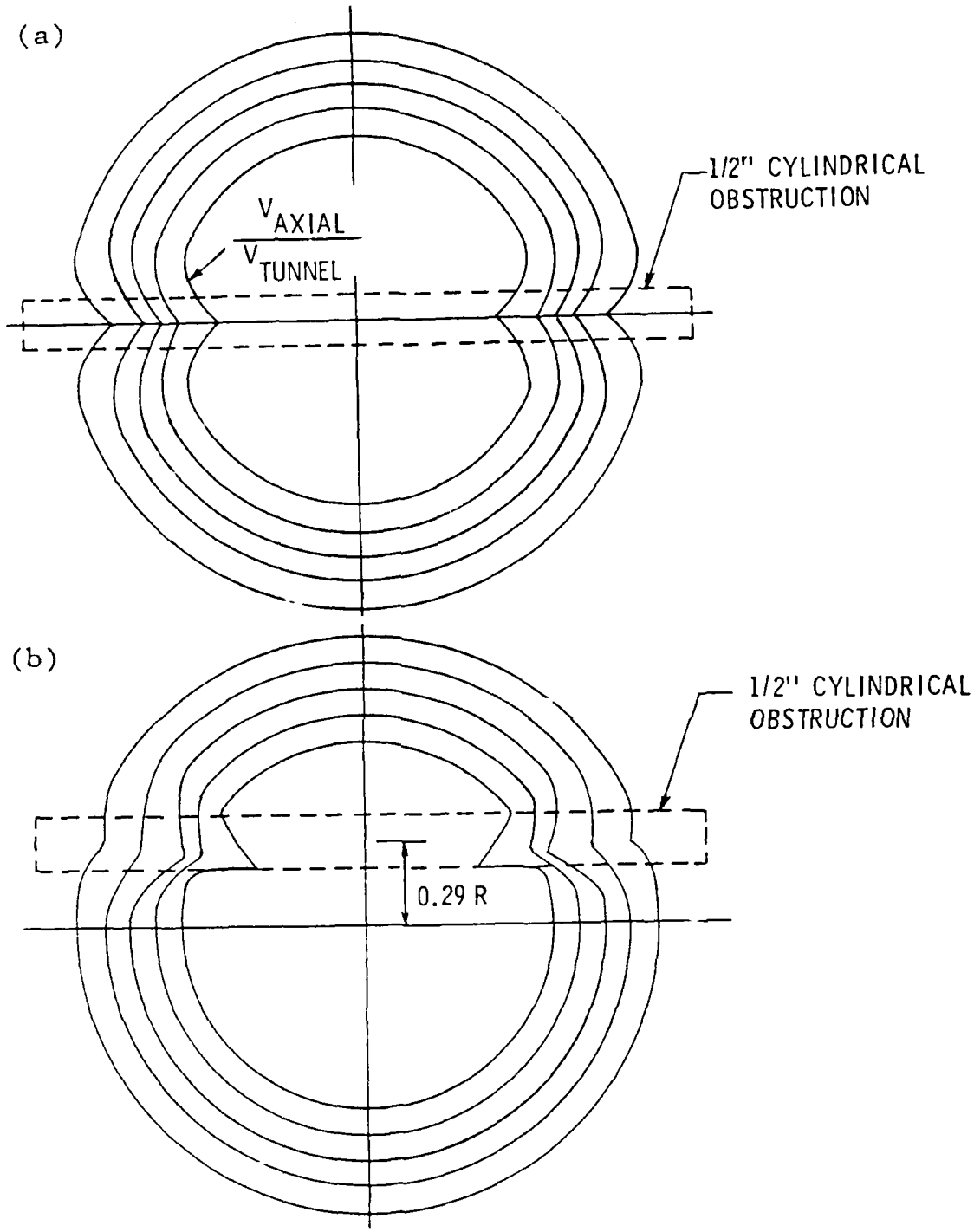


Figure 3.13 Circumferential Distribution of Axial Velocity in the Plan of Blade Leading Edge.
(a) Cylinder at 0.0R
(b) Cylinder at 0.29R
(c) Cylinder at 0.56R
(d) Cylinder at 0.71R

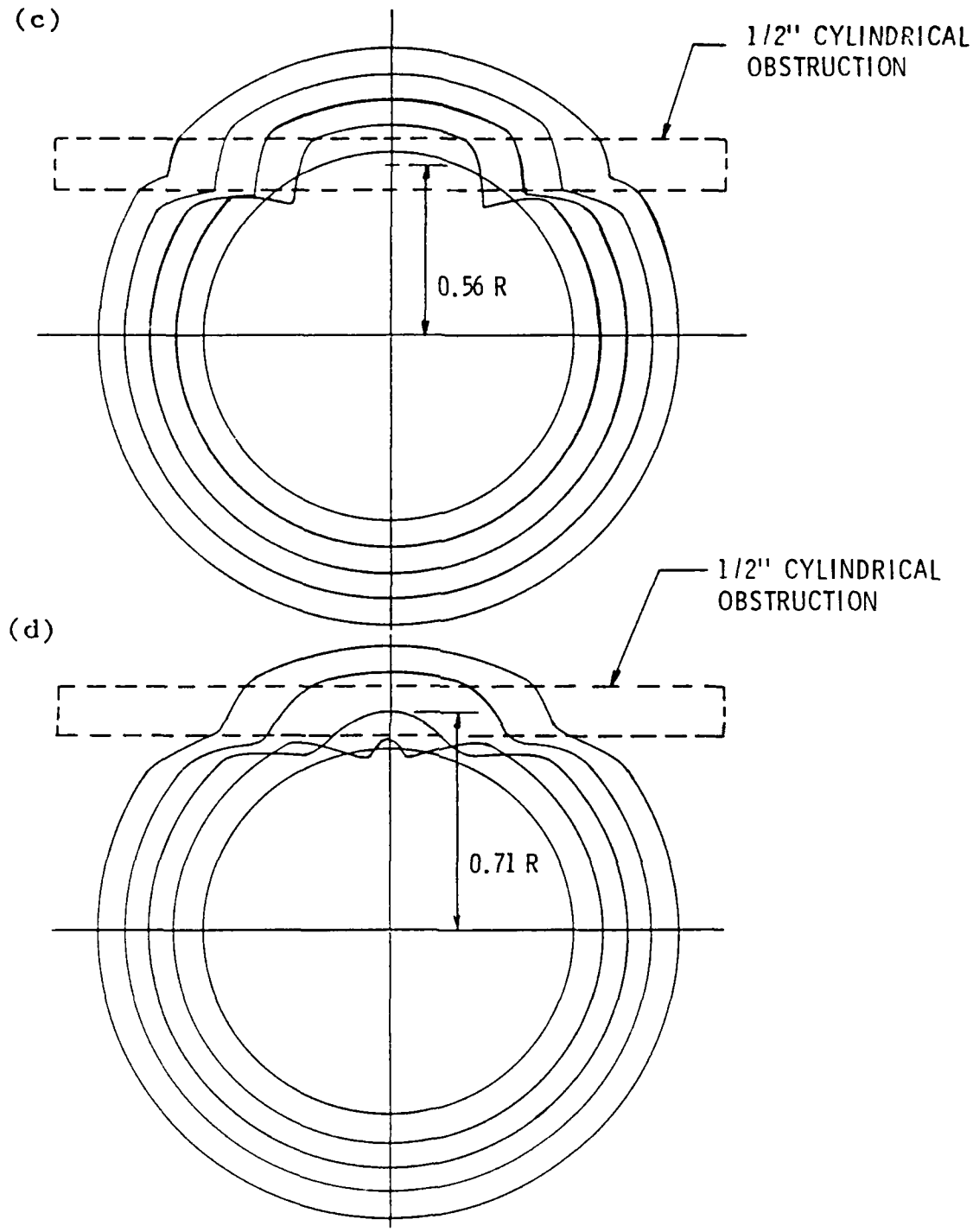


Figure 3.13 (continued)

viscous effects. The wake length is maximum when the cylinder was positioned in front of the center of the fan.

## 3.3 Computation of Discrete-Tone Radiated Sound

### 3.3.1 Fourier Analysis of Inflow Velocity Vector

The inflow velocity $v(r,\theta)$ can be decomposed into circumferential average velocity $\bar{V}(r)$ and a circumferential varying component $\tilde{V}(r,\theta)$:

$$V(r,\theta) = \bar{V}(r) + \tilde{V}(r,\theta) \quad . \tag{3.1}$$

Equation 3.1 can be described by a Fourier series as follows

$$V(r,\theta) = \bar{V}(r) + \sum_{n=1}^{\infty} [a_n(r)\cos(n\theta) + b_n(r)\sin(n\theta)] \quad ,$$

$$= \bar{V}(r) + \sum_{n=1}^{\infty} c_n(r)\cos[n\theta - \phi_n(r)] \quad , \tag{3.2}$$

where

$$V(r) = \frac{1}{2} a_o(r) \quad ,$$

$$a_n(r) = \frac{1}{\pi} \int_{-\pi}^{\pi} V(r,\theta)\cos(n\theta)\, d\theta \quad ,$$

$$b_n(r) = \frac{1}{\pi} \int_{-\pi}^{\pi} V(r,\theta)\sin(n\theta)\, d\theta \quad ,$$

$$c_n(r) = [a_n^2(r) + b_n^2(r)]^{1/2} ,$$

$$t_n(r) = \tan^{-1}[b_n(r)/a_n(r)] ,$$

The phase angle is defined as positive when in the same direction as the blade rotation. For example, the wave $c_n \cos(ng - t_n)$ lags behind $c_n \cos(ng)$ as shown in Figure 3.14. Figure 3.15 presents a typical result of the decomposition using Fourier analysis. This decomposition is for data collected at one fan radius when a cylinder is placed symmetrically in front of the center of the fan. Because the Patriot fan has five (5) blades, the harmonic coefficients at n =5, 10, 15, and 20 will contribute to the unsteady axial force at blade rate and multiples up to 4. Hence, these coefficients were used to compute the unsteady blade loading at the BPF and the first three harmonics. Figure 3.16 (a) shows the magnitude of the harmonic coefficients $C_5$, $C_{10}$, $C_{15}$, and $C_{20}$ at different fan radii. Figure 3.16 (b) shows the corresponding phase. Similar Fourier decomposition was performed for the tangential and radial velocity components, since all three components enter into the unsteady blade loading calculation.

### 3.3.2 The Application of Two-Dimensional, Unsteady Airfoil Theory to the Computation of Unsteady Rotor Force

The axial component of unsteady rotor force caused by rotor blades interacting with a spatially non-uniform, time-invariant inflow was calculated using a two-dimensional unsteady thin airfoil theory [23,

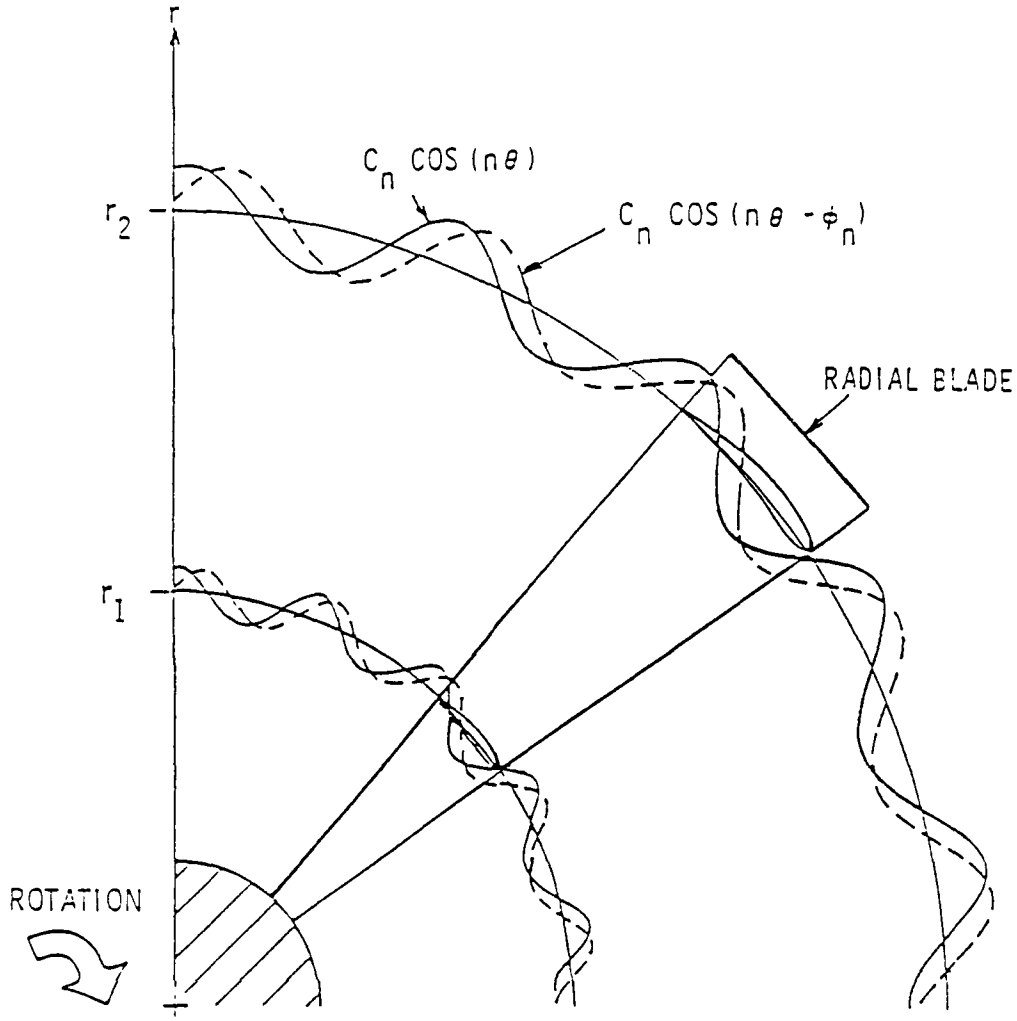


Figure 3.14 The Interaction of a Rotor Blade with Distortions of Different Phase. (The Flow is Coming Out of the Figure and $\theta$ is Positive in the Same Direction as the Blade Rotation) [22].

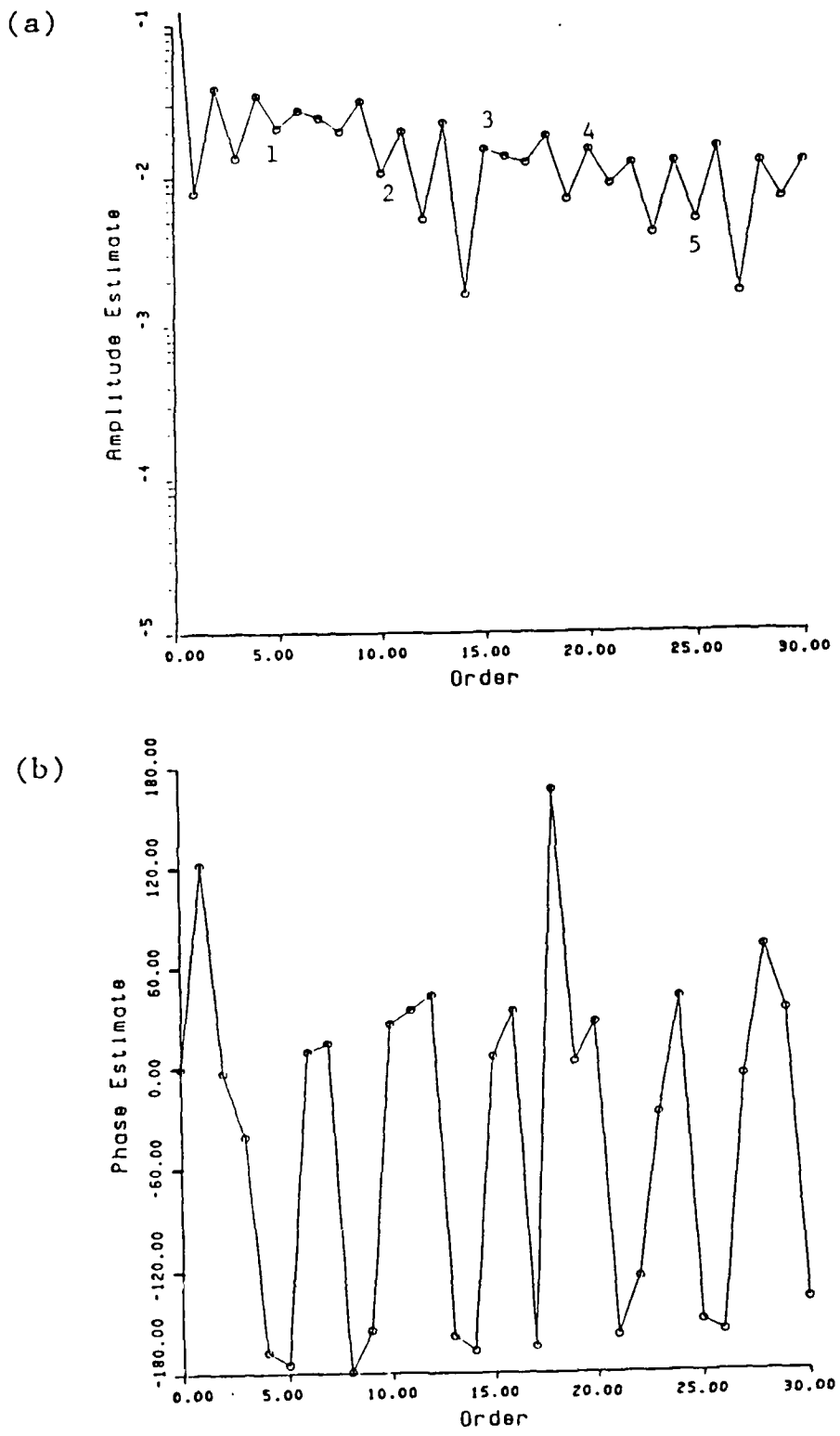


Figure 3.15 Harmonic Content of the Axial Velocity Distributon at One Radial Position
(a) Amplitude
(b) Phase

(a)

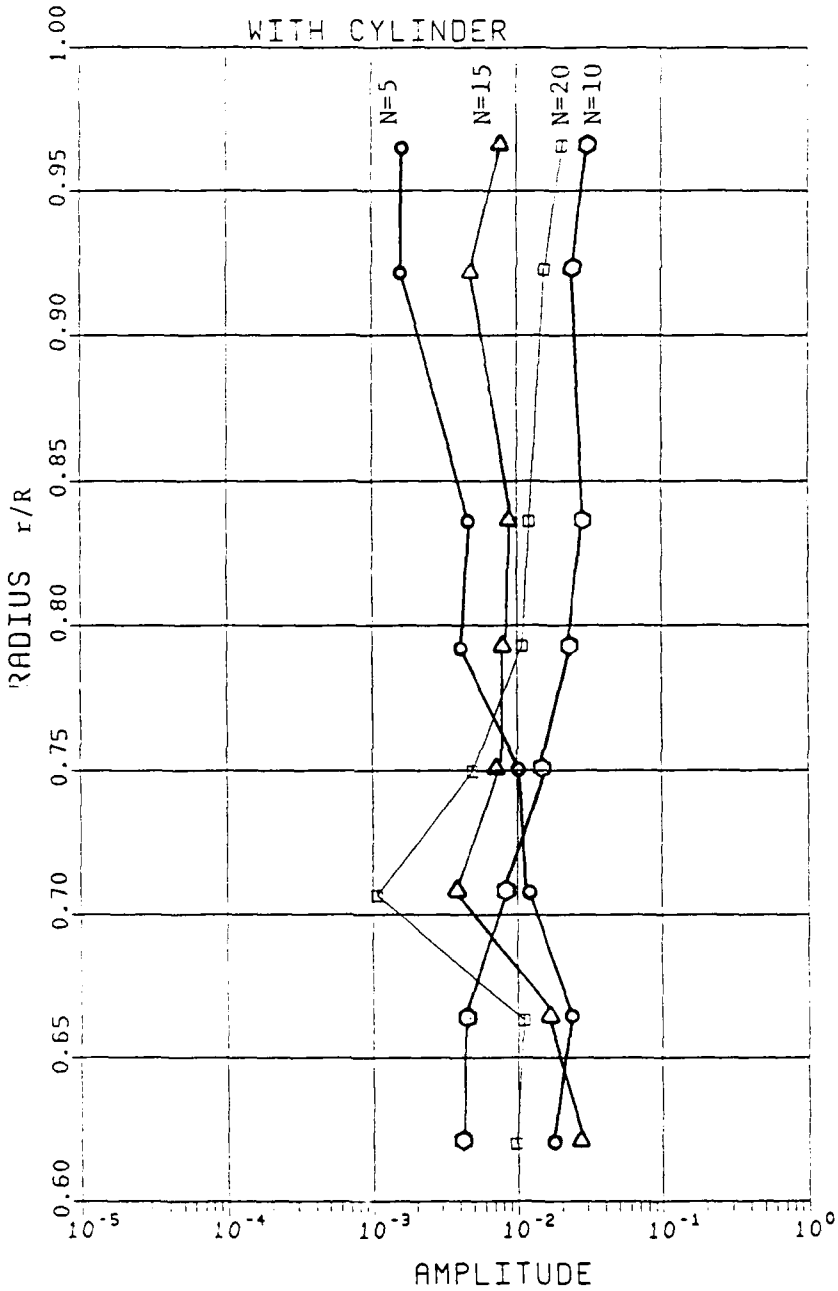


Figure 3.16 Harmonic Content of the Axial Velocity Distribution at Different Radial Positions
(a) Amplitude
(b) Phase

(b)

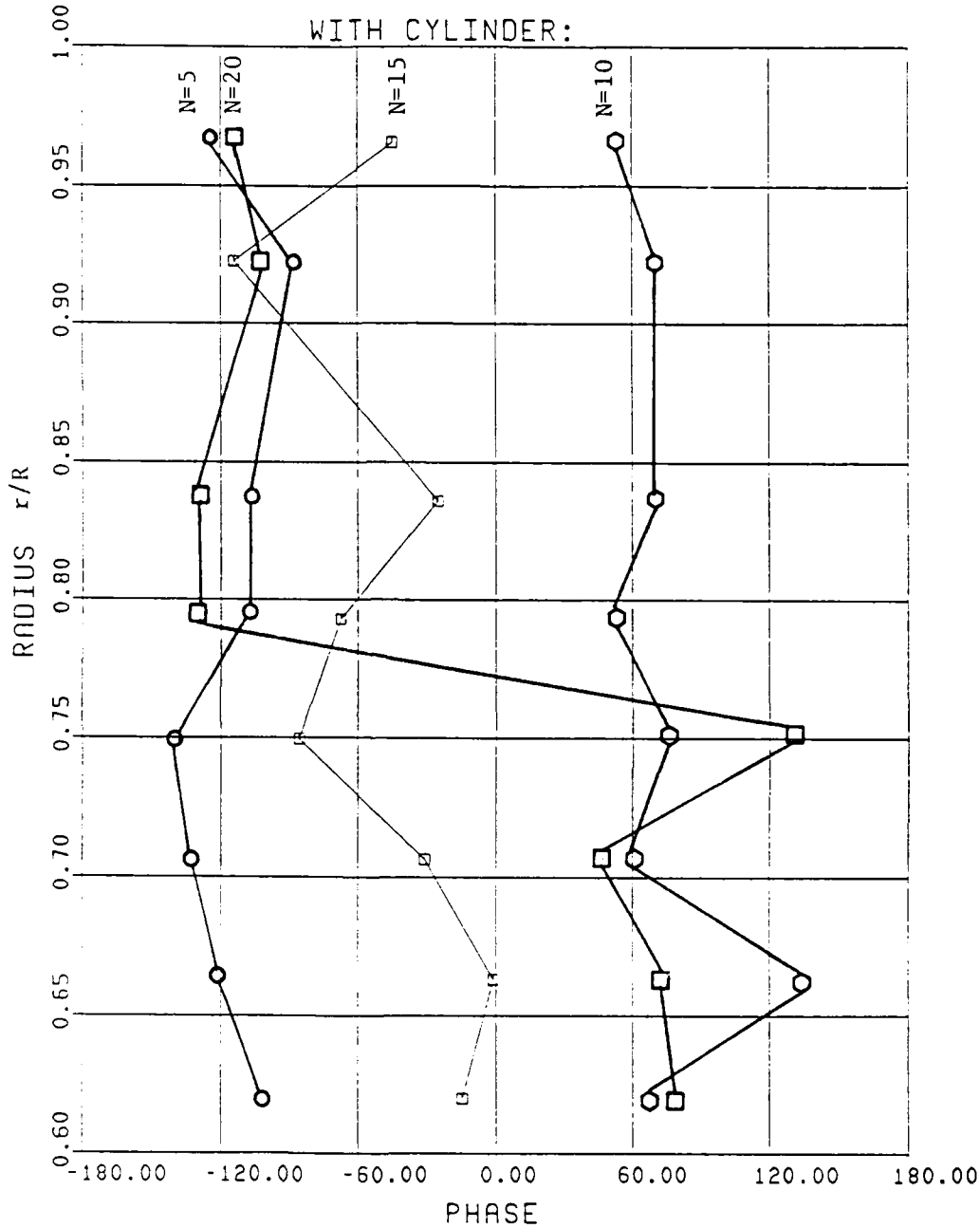


Figure 3.16 (continued)

24, 25]. The rotor blades were assumed to be two-dimensional, isolated airfoils. The airfoil was assumed to be replaced by a vortex distribution as was the wake shed by the airfoil. The unsteady lift on the airfoil was determined for a sinusoidal inflow incident to the airfoil.

For the purpose of computation, the fan blade was divided into nine radial segments. The total unsteady lift on each blade segment due to the nth Fourier component of the inflow was computed using an equation developed by Neumann and Yeh [23], i.e.,

$$\bar{L}_n = \frac{1}{2} \frac{dC_L}{d\alpha} \rho c \bar{W} [\bar{v}_n S (w_n) + \alpha \bar{u}_n F_\alpha (w_n) + \frac{2y_m \bar{u}_n}{c} F_f (w_n)] \quad , \tag{3.3}$$

where

$C_L$ = the steady lift coefficient ,

$\alpha$ = angle of attack on the blade ,

$c$ = blade chord length ,

$\bar{w}$ = circumferential average velocity relative to the blade ,

$y_m$ = maximum camber of the blade ,

$S$ = Sears function ,

$F_f$ = maximum camber function ,

$F_\alpha$ = angle of attack function ,

$\omega$ = $\frac{\nu c}{2w}$ , reduced frequency ,

$\nu$ = angular velocity ,

$u$ = distortion velocity parallel to the relative velocity (w)

and $v$ = distortion velocity normal to the relative velocity (w).

The lift curve slope $dC_L/d\alpha$ should be determined from experimental data that includes cascade effects and airfoil section characteristics at each blade segment.

The axial component of the unsteady lift on the blade segment is

$$\bar{F}_Z(r',t) = -\bar{L}_n \sin(r+\alpha)\cos(\mu) , \tag{3.4}$$

where

$r'$ = distance of the blade segment from the centerline of the fan,

$r$ = stagger angle of the rotor blade ,

$\mu$ = inclination of the streamlines to the axial direction.

The total axial component of the unsteady force acting on the shaft can be obtained by summing the $\bar{F}_Z(r',t)$ vector over all radial segments and over all blades, i.e.,

$$F_Z(t) = -B \sum_{r'=r_H}^{r_t} |\bar{L}_n| \sin(r+\alpha)\cos(\mu)\, e^{i(n\Omega t + \Phi_n)} . \tag{3.5}$$

Here, one has $\Omega$ = angular velocity of the blade ,

$B$ = number of blades ,

$r_H$ = hub radius ,

$r_t$ = blade tip radius ,

and $\Phi_n$ = unsteady lift phase angle on reference blade .

The unsteady rotor force at the BPF and its harmonics can be computed from the inflow harmonics corresponding to these frequencies using equation 3.5. A CFD package which implements this methodology has been developed by Zierke at Penn State University [22]. The predictions using this computational code have been compared with experimental results from other experiments. These comparisons showed that the

predictions gave the correct trend of unsteady forces as various parameters were changed [22]. However, the method can not always be expected to give the correct magnitudes of the unsteady blade forces due to the assumptions made in the calculation [22].

### 3.3.3 Theoretical Development for Correlating Unsteady Rotor Force and Discrete-Frequency Noise

The correlation between blade surface fluctuating loading and farfield acoustic pressure can be determined by using Curle's generalized solution of the Lighthill equation [26, 27]. Several assumptions which are appropriate for the small axial flow cooling fan used in this study were used to simplify Curle's equation [28, 29]. These assumptions are as follows:

1. The Mach number of the blade tip is low.
2. the blade surface is in rigid steady motion.
3. The total blade force is dominated by the normal component.
4. The sound wave-length is larger than the dimension of the fan, i.e. the fan is a compact source.

The simplified Curle's equation [28, 29] correlates the unsteady rotor force to the radiated noise and is given by:

$$P\ (r,t) \simeq \frac{\cos\theta}{4\pi r}\left(\frac{\partial F}{\partial t}\right) , \tag{3.6}$$

or

$$P\ (r,f) \simeq \frac{fF(\cos\theta)}{2r\ c_o} , \tag{3.7}$$

where

$c_o$ - the ambient speed of sound ,

F - unsteady rotor force ,

f - frequency ,

r - the distance between fan and field point ,

and $\theta$ - the angle between fan axis and field point .

The farfield acoustic pressure is proportional to the time rate of change of the unsteady rotor force. This equation uses the point-loading concept, i.e. the net integral blade loading is considered to be acting at an effective point on the rotor disk. This equation is only valid when the fan is a very compact source.

### 3.3.4 Computational Procedure, Results and Discussion

In this study, the procedures for computing the discrete-frequency radiated sound caused by the interaction of fan blades and a periodic non-uniform inflow are summarized as follows:

1. Measure the three-dimensional velocity vectors in the blade plane using five-hole probes. The five-hole probes were positioned at nine fan radii and rotated 360° in 3° increments. Therefore, the circumferential velocity distribution at nine fan radii in the blade plane was determined. There are 120 data points for each circumferential velocity distribution at each fan radius.

2. Calculate the harmonic coefficients of the velocity vectors at each fan radius using equation 3.2.
3. Measure the blade geometry parameters which include pitch, camber, thickness, skew, rake, and stagger angle at each radial segment or strip location. The blade was divided into nine segments, corresponding to the radii for which there is experimental velocity data.
4. Compute the rotor unsteady axial force at the BPF and its harmonics using the CFD package which implements equations (3.3), (3.4), and (3.5). The harmonic coefficients of the velocity vectors at the nine fan radii and the blade geometric parameters obtained in step 2 and 3 are the inputs for this computation.
5. Compute the discrete-frequency radiated sound from the unsteady rotor forces using equation (3.7).

The unsteady rotor force and the discrete-frequency radiated sound were computed for the case of a cylinder in front of the center of the fan. The computed unsteady rotor forces are 0.0545N, 0.0260N, 0.0240N, 0.0337N for the BPF and the first, second, and third harmonics. The computed discrete-frequency radiated sound and its comparison to the measured values are shown in Table 1. The experimental results were obtained using synchronous time averaging as described in section 4.3. The computational and experimental results agree quite well at the BPF and the first harmonic, while for the third and fourth harmonics the agreement is poorer. This could possibly be due to the fact that the fan is a less compact source at the second and third harmonics (575 Hz

Table 1. The Discrete Tones Radiated by the Patriot Fan with a 1/2" Cylindrical Obstruction in the Inlet Flow

On-Axis SPL of the BPF Harmonics, dB re 20 μPa

| | BPF | BPF X 2 | BPF X 3 | BPF X 4 |
|---|---|---|---|---|
| Experimental Result | 58.2 | 62.9 | 45.8 | 45.3 |
| Computational Result | 61.2 | 60.7 | 63.7 | 69 |

and 760 Hz, respectively). The ratio of wave length to fan diameter at the second and third harmonics are 2.2 and 1.7 respectively. The simplified Curle's equation breaks down rapidly as the acoustic wavelength becomes smaller and smaller relative to the fan diameter.

# Chapter 4

# MODIFICATIONS AND ACOUSTIC EVALUATIONS OF DUCT INLET AND FINGER GUARD

## 4.1 Introduction

The interaction between time invariant circumferentially non-uniform inflow and the blades causes unsteady blade forces and discrete-frequency noise. Therefore, reduction of the discrete-frequency noise can be achieved by reducing the inflow distortion. Methods by which this can be done include: improving the circumferential symmetry of the rotor annulus inlet and avoiding the blockage of the upstream flow field.

The finger guard is a necessary safety device on a fan. It is also one of the major sources of inflow distortion. Gray [30] and Filleul [4] showed that significant sound is radiated from the 90% span region of the rotor, which is very near the shroud. The uniformity of the inflow field in the vicinity of the shroud is therefore critical and influenced by the duct inlet. The duct inlet and finger guard of the patriot fan were modified in an attempt to reduce the discrete-frequency noise. The acoustic evaluations for the modified duct inlet and finger guard prototype configuration were conducted in the "air-breathing" anechoic chamber as described in section ?... Evaluation results and conclusions are presented in this chapter.

## 4.2 Modifications of Duct Inlet and Finger Guard

The design modifications for the duct inlet and finger guard were based on Washburn's recommendations [18]. These are as follows:

1. Aerodynamic shaping of unavoidable inflow obstructions such as finger guards.
2. The identification of a minimum distance of 0.3 fan radius for the placement of the finger guard.
3. The avoidance of any blockage in the lateral flow.
4. The possible use of an inlet baffle that can help to accelerate the edge flow and hence reduce the inflow distortion.

The redesigned duct inlet (baffle) and finger guards are shown in Figs. 4.1 and 4.2. The finger guard was attached to the baffle.

The baffle inlet begins at the edge of the fan inlet housing. It then sweeps smoothly back from the inlet to a height which would accommodate the bolts which mount the baffle to the fan. The baffle remains at this height over a radial distance equal to one radius of the fan rotor and it is tapered back to the wall as shown. The finger guard was made from small wire to reduce the blockage to the inflow field. The finger guard consists of circular and leaned radial members. The symmetric circular members are not expected to cause unsteady blade force and resultant discrete-frequency noise. The interaction between blades and the wakes, generated by the radial members is periodic and can contribute to discrete-frequency noise at

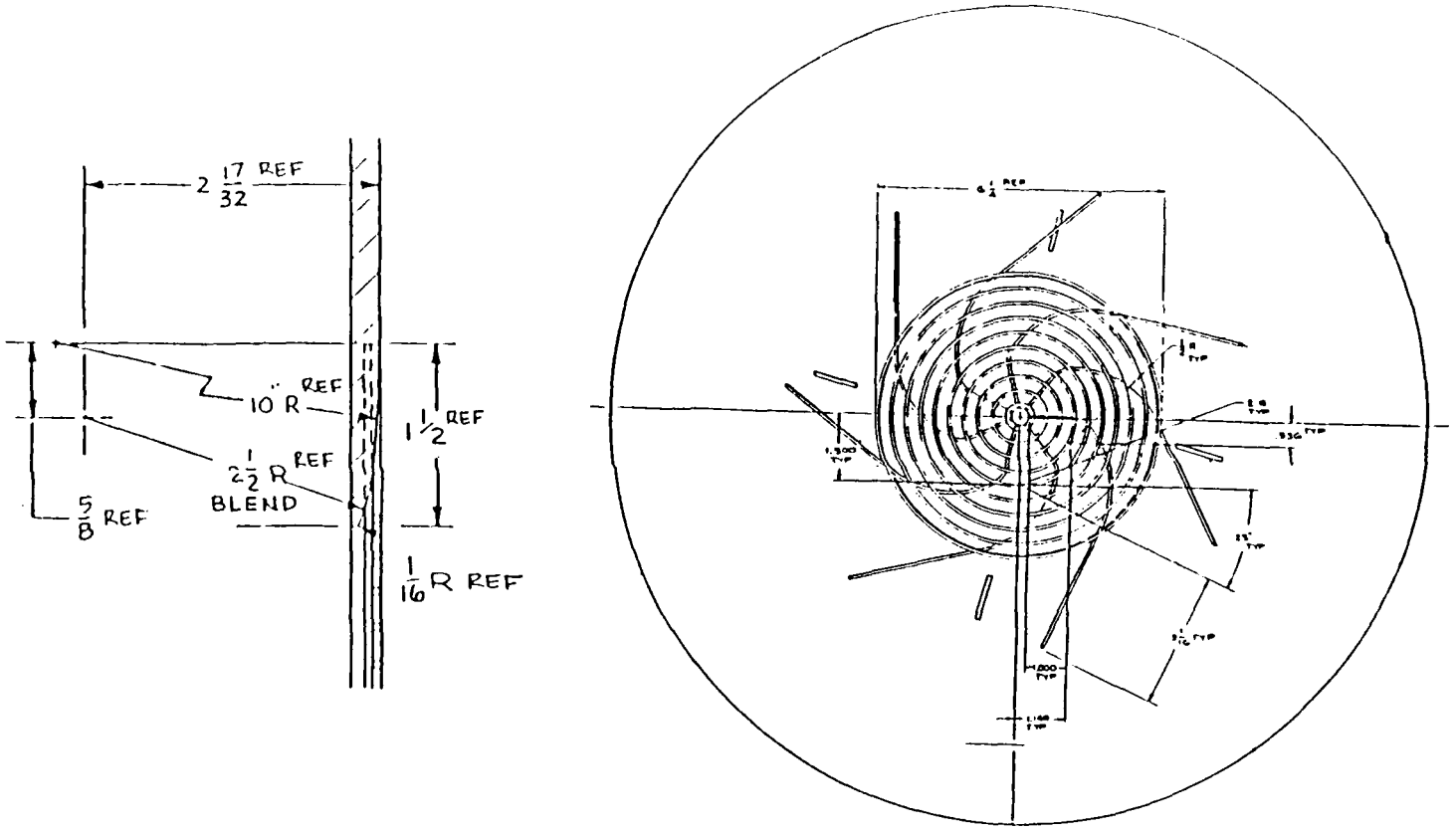


Figure 4.1 Redesigned Duct Inlet and Finger Guard.

(a)

(b)

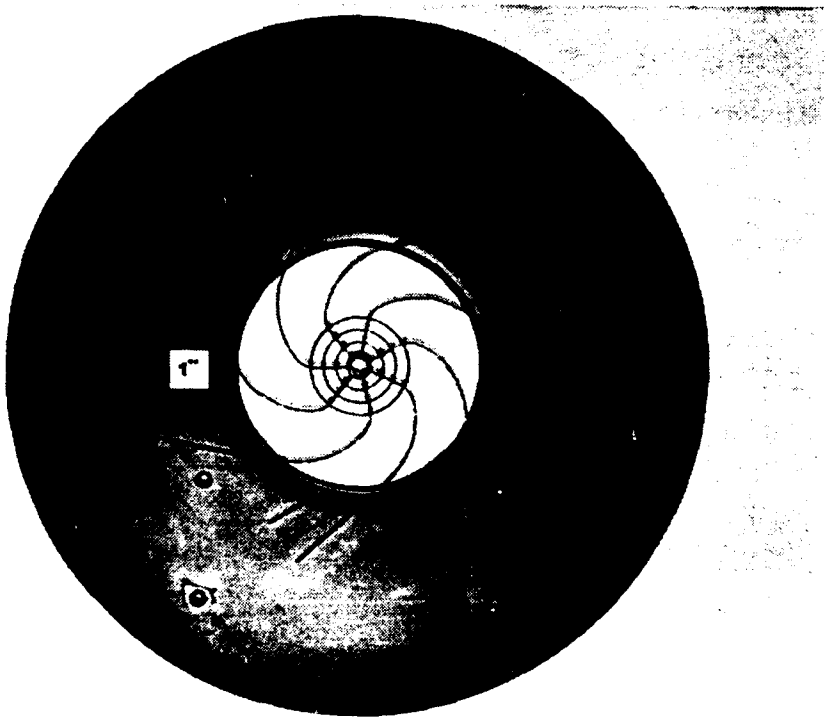

Figure 4.2 Appearance of Modified Duct Inlet and Finger Guards.
(a) Four Radial Members (b) Seven Radial Members

multiples of the Blade Passage Frequency (BPF). Curle's equation shows that the fan radiated noise is proportional to the time rate of change of the unsteady blade force. Experimental results [31] indicate that the more nearly parallel a shed vortex is to the blade leading edge during the interaction between blade and vortex, the greater the radiated sound. A perpendicular interaction between a blade leading edge and upstream strut shed vortex results in the least discrete-frequency noise. The leaned radial members are such that they cross the blade leading edge at an angle and pass by only a small portion of the blade leading edge at any one time, i.e., reduce the time rate of change of the unsteady blade force. The unsteady blade force and the radiated tonal noise will thus be expected to be reduced. Finger guards with 4 and 7 radial members were used in order to investigate the effect of the number of radial members on the discrete-frequency radiated noise of a fan with 5 blades. Fig. 4.2 shows the prototype configurations of a baffle and finger guard with some of the circular members omitted. There is a round plate at the center of the original finger guard which is used on the Patriot fan. It blocks and distorts the inflow; therefore, this center plate was removed as shown in Fig. 4.3 in order to evaluate the effect of the center plate on the radiated noise. Fig. 4.4 shows the original finger guard and the final redesigned version.

In the final redesigned finger guard, the center plate of the original finger guard was replaced by round wire to reduce the inflow blockage. The spiral radial members were designed so that they cross the blade leading edge at a greater angle than was the case for the

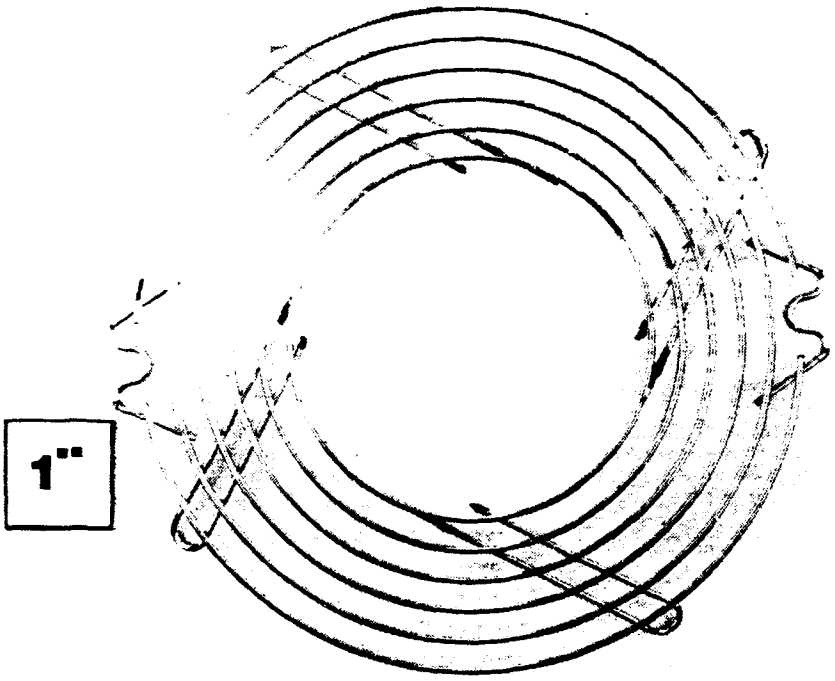


Figure 4.3 Appearance of Modified Finger Guard Without Center Plate.

(a)

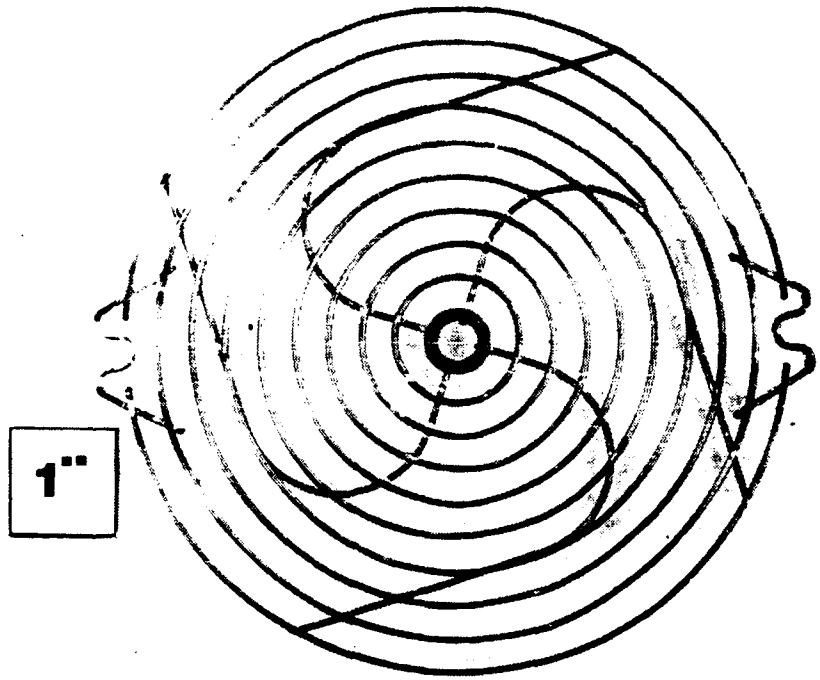


(b)

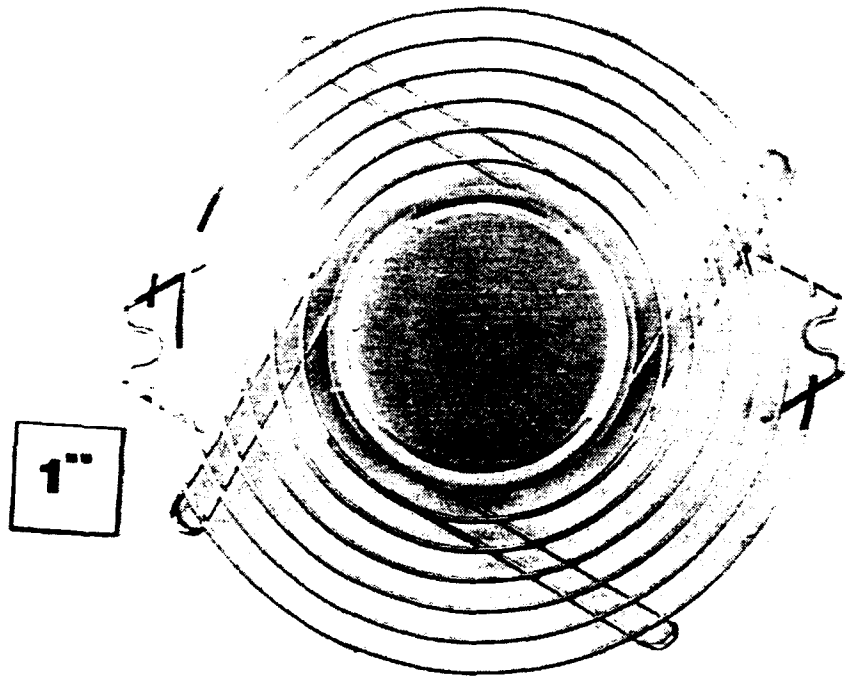


Figure 4.4 Appearance of Redesigned and Original Finger Guards
(a) Redesigned Finger Guard
(b) Original Finger Guard

original finger guard. This reduces the interaction between the radial member wake and blade at the time when the blade passes through the radial member wake.

## 4.3 Experimental Setup

The acoustic evaluation of the modified inlet duct and fingerguard prototype configurations was conducted in the "air-breathing" anechoic chamber as described in section 2.2. A B&K type 4220 2.54 cm microphone was positioned on the fan axis at a distance 1 m away from the fan. During the tests, the sound pressure level (SPL) of the discrete-frequency noise was measured using synchronous time averaging [18] to enhance the rotational tones relative to the random, non-rotational broadband noise. A fotonic sensor was positioned behind the rotor. It supplied a pulse signal at the blade passage rate to trigger the spectral analyzer to take acoustic data from the microphone. The acoustic data was thus taken in a time period which started at a time when the system was physically identical to the previous period. All data which is not phase coherent with the blade rate tends to be averaged to zero. Figure 4.5 shows the flow schematic for the measuring system. Figure 4.6 is a photograph of the experimental setup.

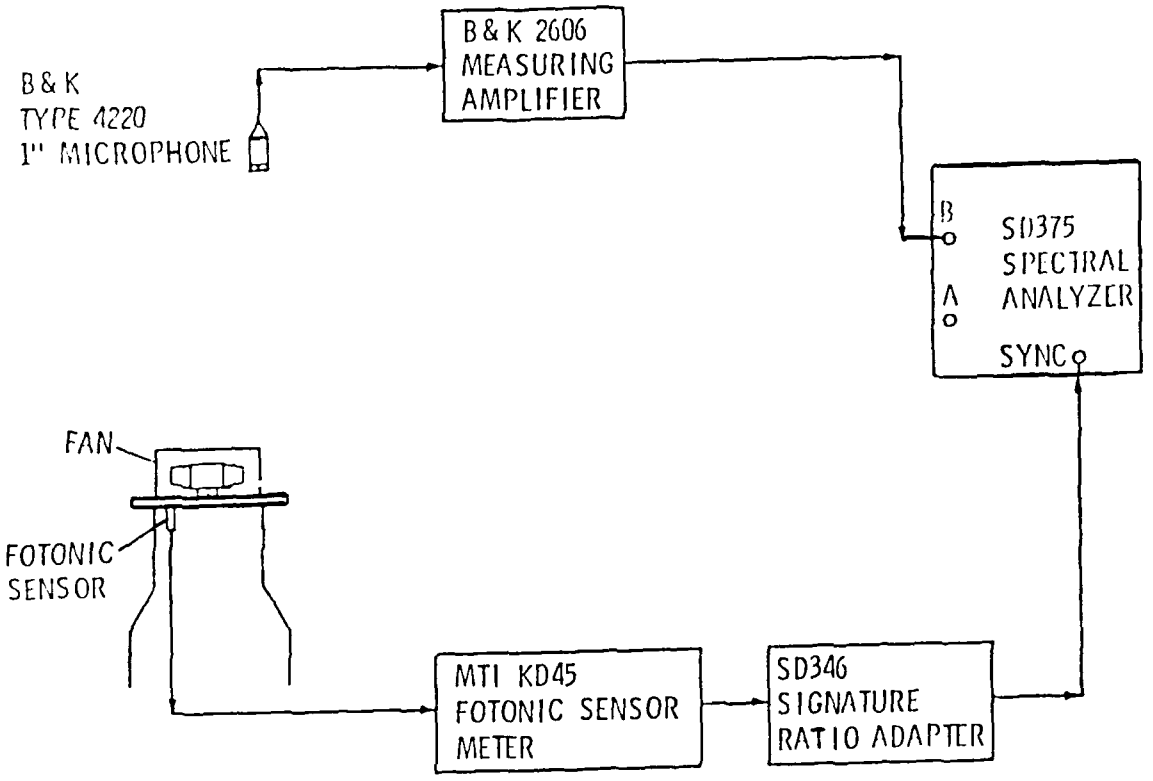


Figure 4.5 Flow Schematic for the Measuring System.

(a)

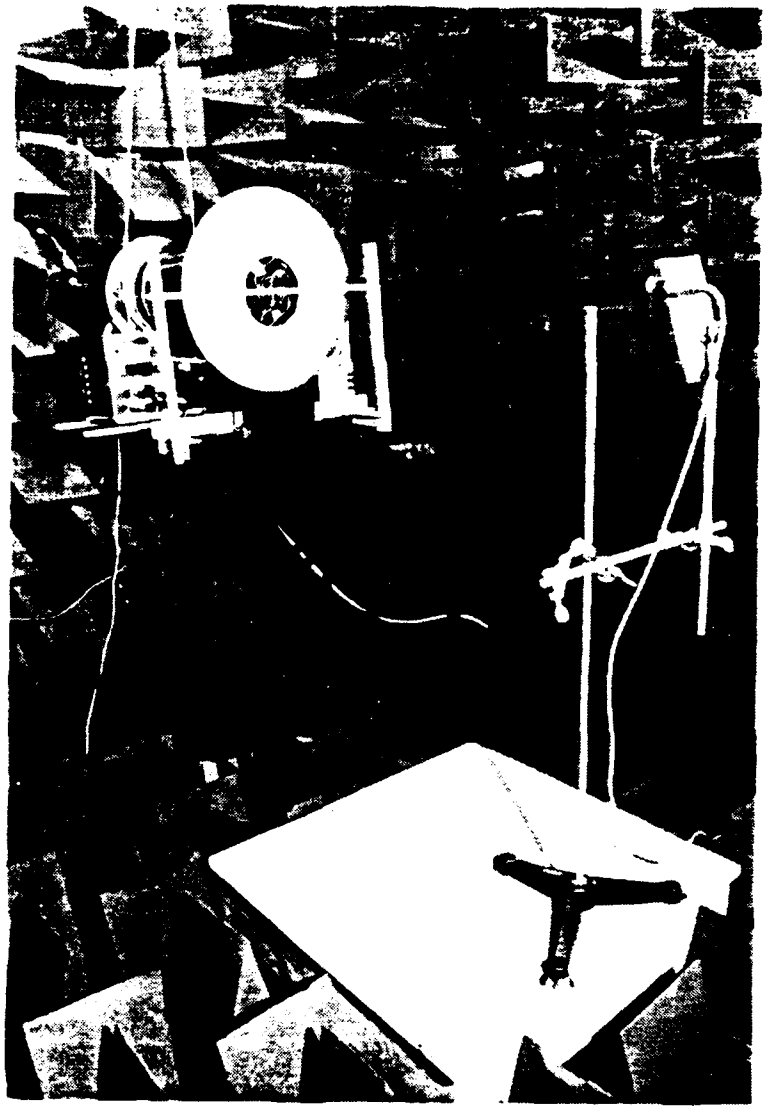

Figure 4.6 Photograph of Experimental Setup
(a) Inside the Anechoic Chamber. Included are a patriot fan, modified fan inlet (baffle), and a microphone on its mount and stand
(b) Fan Exhaust Duct and Throttle

(b)

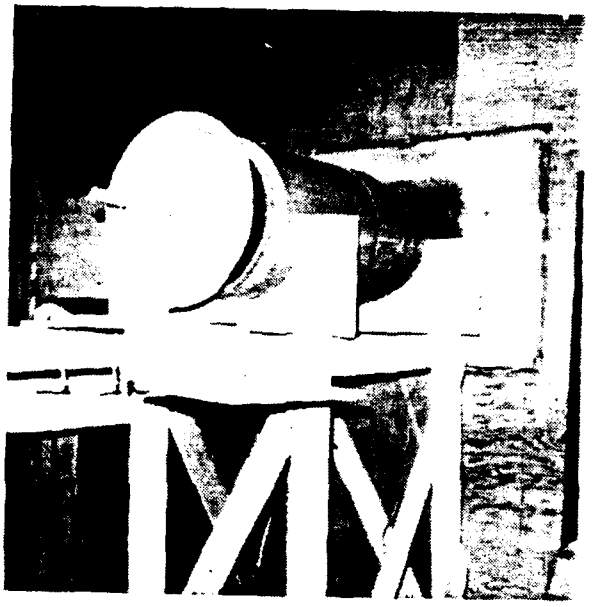

Figure 4.6 (continued)

## 4.4 Acoustic Evaluations and Conclusions

Fig. 4.7 shows the sound spectrum of the Patriot fan tested with and without a cylindrical obstruction in front of the fan. The discrete-frequency noise occurs mainly below 2000 Hz. The test frequency range was therefore chosen from 0 to 2000 Hz for the entire evaluation process. The following results are for the Patriot fan without cylinder.

The inclusion of the baffle causes an increase in discrete-frequency noise at the BPF and BPF X 2 by 5 dB and 3 dB, respectively as shown in Fig. 4.8(b). The baffle was not helpful in reducing the discrete-frequency noise. The original duct inlet of the Patriot fan is a good design and can effectively smooth the inlet flow surrounding the shroud. The baffle was also offset from the axis by 0.18 cm to examine possible changes in the discrete-frequency noise due to asymmetry. The offset baffle causes the blades to experience periodic unsteady forces due to the asymmetry of the circumferential inflow field. Fig. 4.8(c) shows a significant increase at BPF X 2 and BPF X 4 as expected. It indicates that the uniformity of inflow field around the blade tip region is critical in discrete-frequency noise reduction.

Figure 4.9 presents the synchronized sound spectra for a baffled Patriot fan with four and seven radial members. It shows that the fan operating with a finger guard with four radial members is slightly quieter than the one with seven radial members. Therefore, the final version of the redesigned finger guard has four radial members as shown in Fig. 4.4(a).

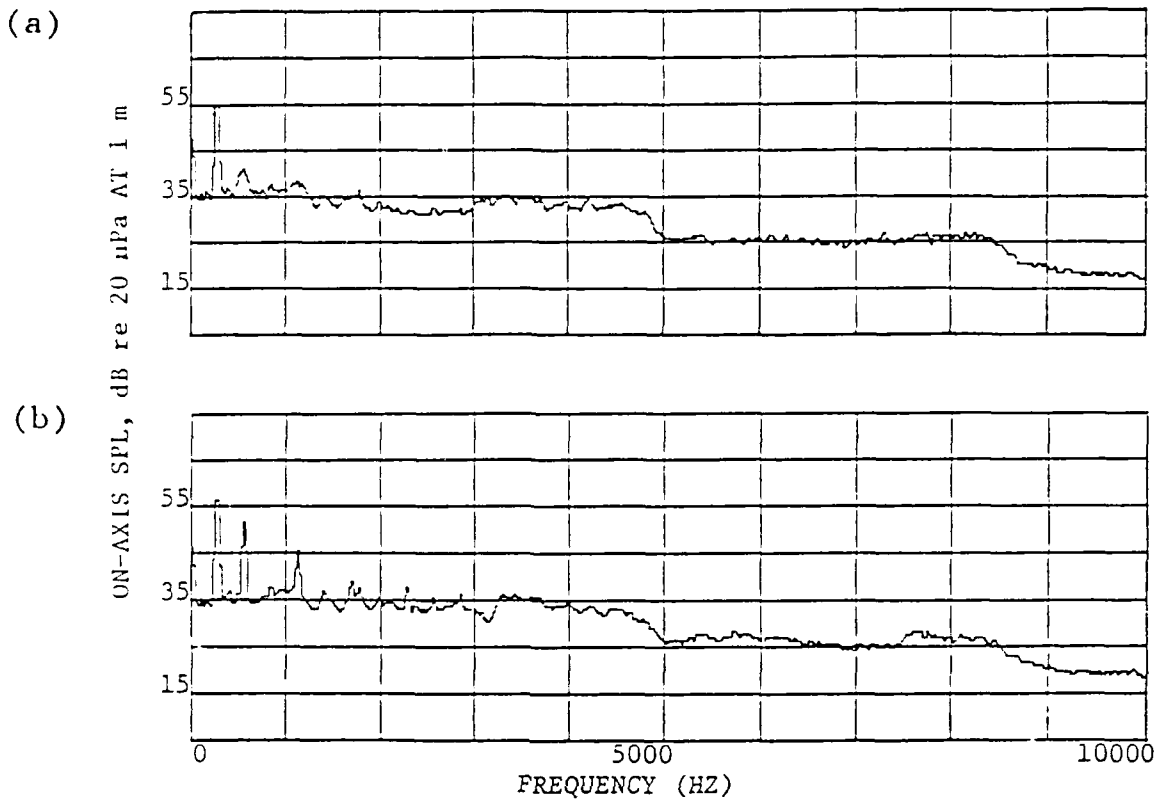


Figure 4.7 Unsynchronized Spectra of Sound Pressure of Patriot Fan.
(a) No Obstruction
(b) 1/2" Cylindrical Obstruction in the Inlet Flow

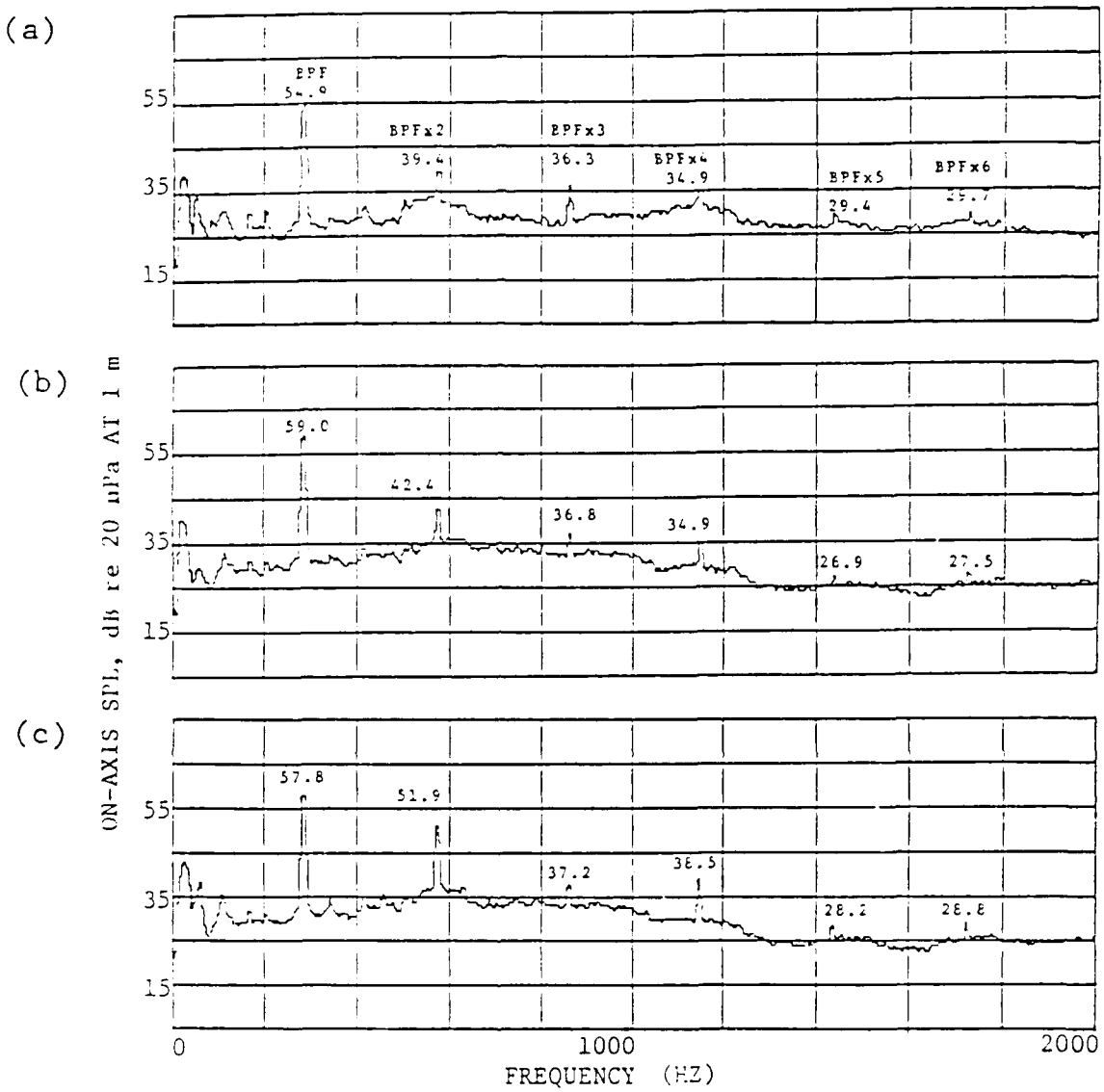


Figure 4.8 Unsynchronized Spectra of Sound Pressure Without Cylinder
(a) No Baffle
(b) Baffle
(c) Baffle Offset 1/10"

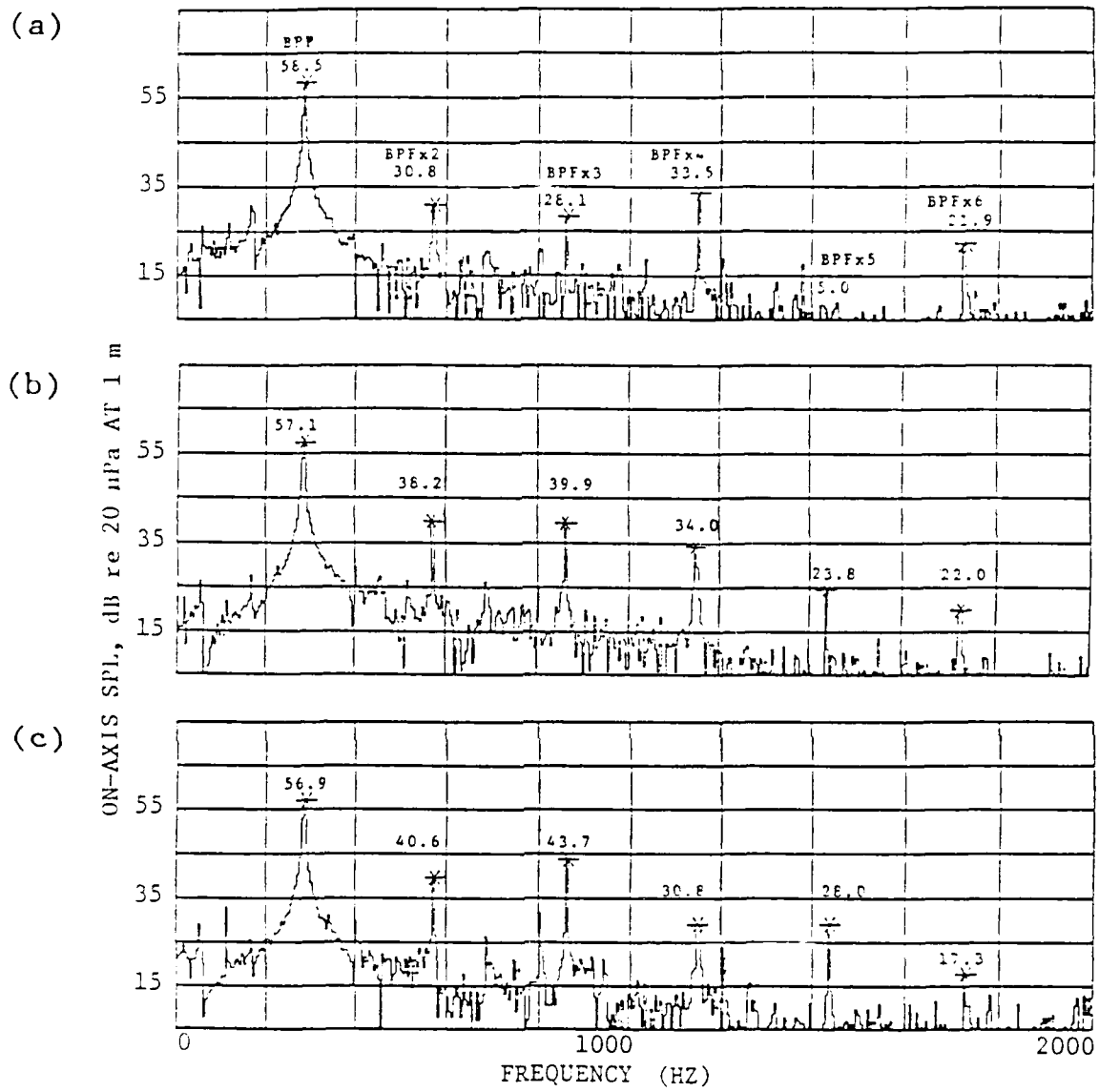


Figure 4.9 Synchronized Spectra of Sound Pressure of Patriot Fan
(a) Baffle
(b) Baffle and Finger Guard with Four Radial Members
(c) Baffle and Finger Guard with Seven Radial Members

Figures 4.10 and 4.11 and Tables 2 and 3 present the evaluation results which involve: the original finger guard, the original finger guard without center plate, and the final version of the redesigned finger guard. Table 2 shows the changes of the discrete tones obtained from the synchronized spectra shown in Fig. 4.11. The differences in SPL observed between unsynchronized spectra (Fig. 4.10) and synchronized spectra (Fig. 4.11) were due primarily to the broadband noise situated at these frequencies. The broadband (random) noise was averaged out in synchronized spectra.

A comparison between the original and the redesigned finger guards shows that the redesigned one has lower BPF, and BPF X 4 tones, but has higher BPF X 2, BPF X 3 and BPF X 5 tones. The changes in SPL at the BPF and its first three harmonics are not significant as shown in Table 2. It is not surprising since the original and redesigned finger guard utilize the same design philosophy. The overall sound pressure levels (OASPL) and A-weighted levels were examined and shown in Table 3. Again the change in OASPL is minor.

The original finger guard was then modified by removing the center plate. The center plate apparently blocks a significant part of the inflow field. The OASPL doesn't show significant change but the discrete tones at BPF X 3 and BPF X 4 were reduced by 6 and 11 dB, respectively.

It is concluded that the original duct inlet is effective in smoothing the inflow surrounding the shroud. An additional baffle does not help in reducing discrete-frequency noise. The redesign of the finger guard was based on a design philosophy which is: the more

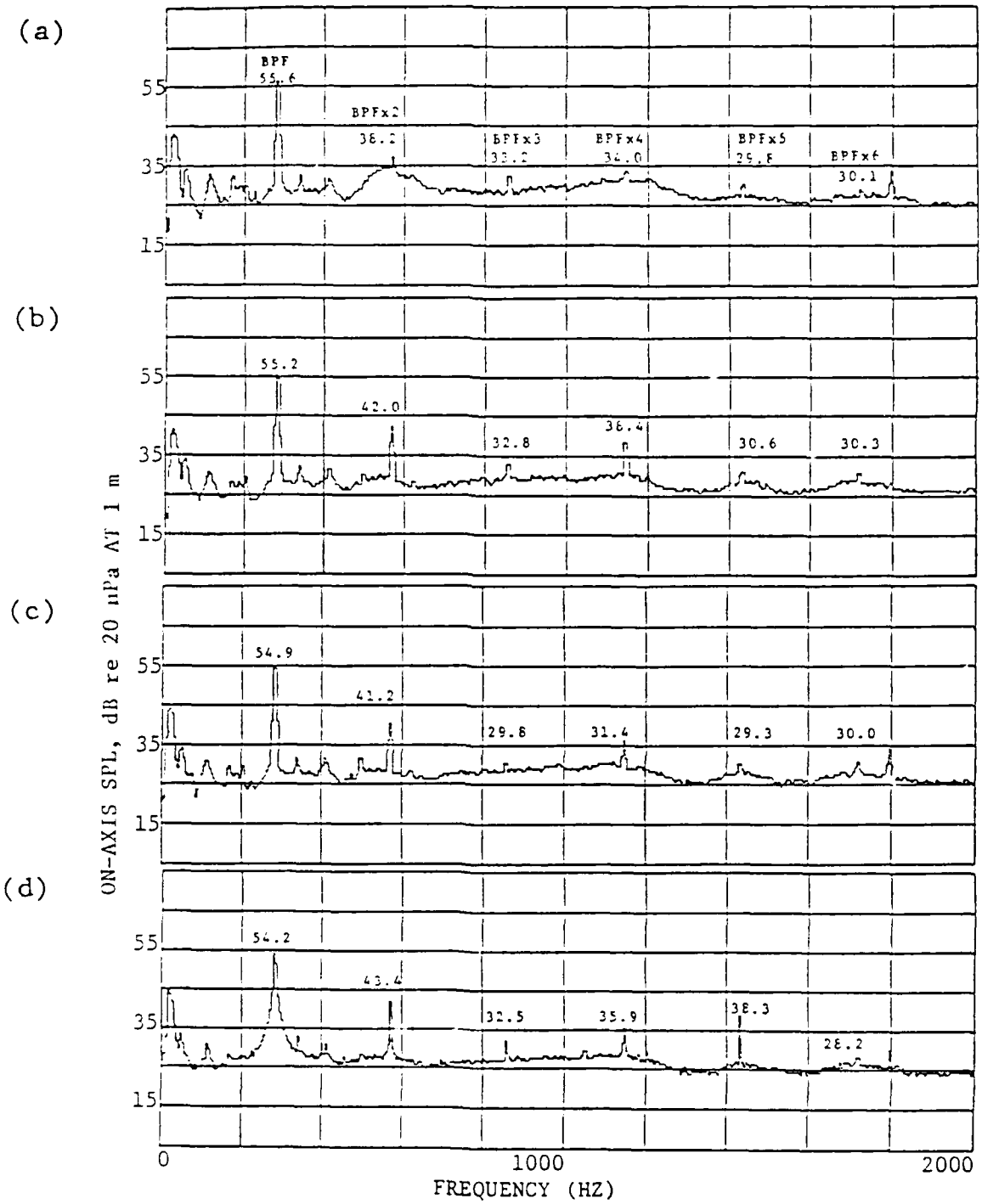


Figure 4.10 Unsynchronized Spectra of Sound Pressure of Patriot Fan.
(a) No Obstruction
(b) Original Finger Guard
(c) Original Finger Guard without Center Plate
(d) Redesigned Finger Guard

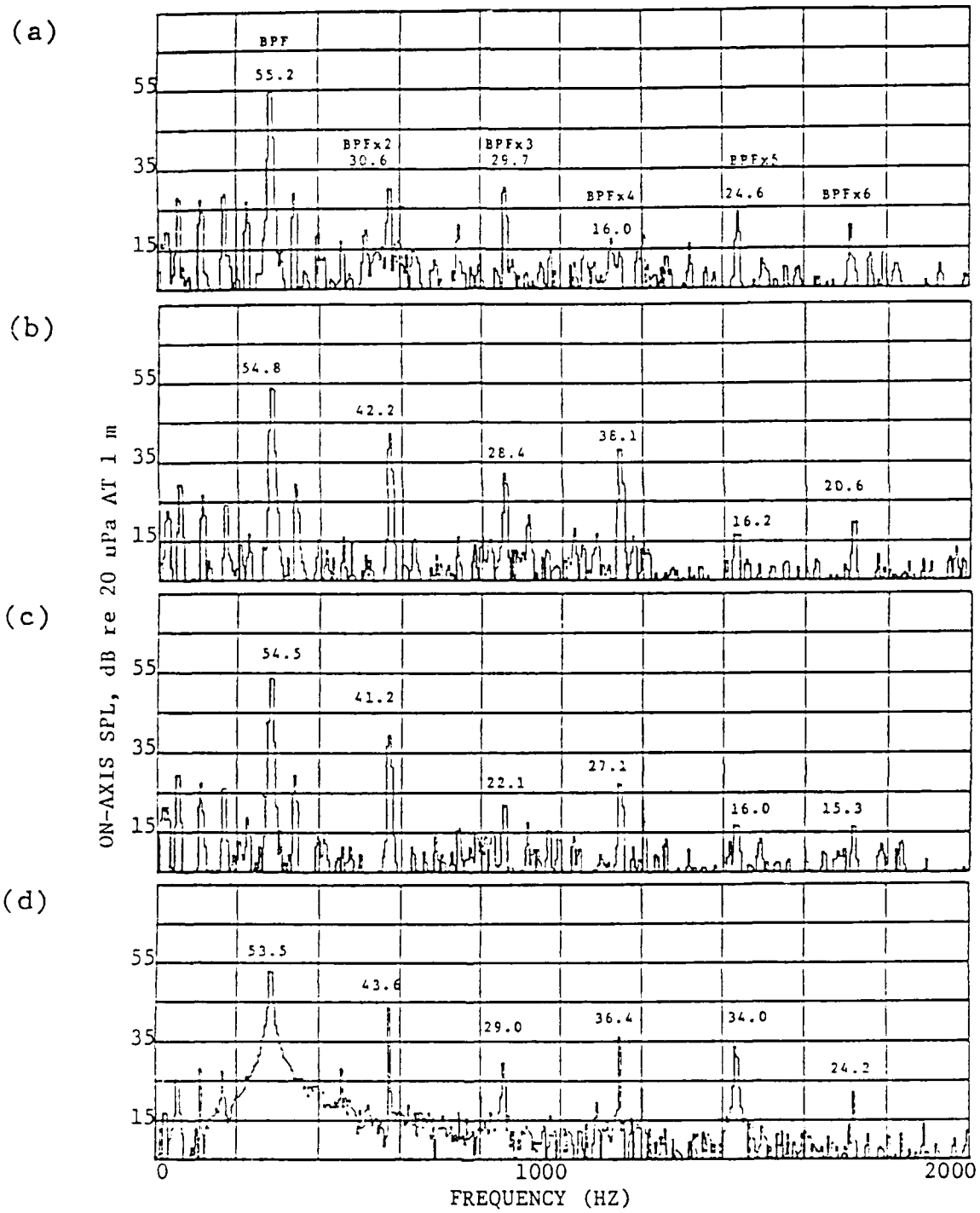


Figure 4.11 Synchronized Spectra of Sound Pressure of Patriot Fan.

(a) No Obstruction
(b) Original Finger Guard
(c) Original Finger Guard without Center Plate
(d) Redesigned Finger Guard

Table 2. Effects of the Finger Guard on the Discrete Tones Radiated by the Patriot Fan

Condition Changes in the On-Axis SPL of the BPF Harmonics, dB re 20 $\mu$Pa from a Unobstructed Fan

| | BPF | BPFX2 | BPFX3 | BPFX4 | BPFX5 | BPFX6 |
|---|---|---|---|---|---|---|
| Original Finger Guard | -0.4 | 11.6 | -1.3 | 22.1 | -8.4 | -0.5 |
| Original Finger Guard without Center Plate | -0.7 | 10.6 | -7.6 | 11.1 | -8.6 | -5.8 |
| Final Phase of Redesigned Finger Guard | -1.9 | 13 | -0.7 | 20.4 | 9.4 | 3.1 |

Table 3. Overall Sound Pressure Level for Tested Patriot Fan

| Condition | dB re 20 μPa | dBA re 20 μPa |
|---|---|---|
| No Obstruction | 57.1 | 55 |
| Original Finger Guard | 57.2 | 55.5 |
| Original Finger Guard without Center Plate | 57.0 | 55.2 |
| Final Phase of Redesigned Finger Guard | 57.6 | 56 |

nearly perpendicular the radial member is to the blade leading edge, the less the discrete-frequency radiated noise. The original factory-design finger guard attempted to accomplish this. The greater angle between radial members and blade leading edge of the the redesigned finger guard did not show significant noise improvements over the original one. The arrangement of the radial members in both the original and redesigned finger guard appears to be optimum. The center plate of the original finger guard blocks part of the inflow which causes discrete-frequency noise. The original finger guard can be improved by replacing the center plate with circular members in order to avoid the inflow blockage.

# Chapter 5

# CONCLUSIONS AND RECOMMENDATIONS

## 5.1 Summary and Conclusions

The correlation among the non-uniform inflow, the unsteady blade force, and the discrete-frequency radiated noise of a small axial-flow cooling fan was studied quantitatively. The fan inlet and the finger guard were modified and evaluated acoustically in an attempt to reduce the tonal noise.

The discrete-frequency noise at the BPF and harmonics is a result of fluctuating blade forces which are caused by the interaction of the blades and time invariant spatially non-uniform inflow. The simplified Curle's equation for compact sources shows that the farfield acoustic pressure generated by an axial flow fan is proportional to the time rate of change of unsteady rotor axial force. To measure the unsteady blade loading of the Patriot fan, a two-layer piezoceramic transducer was designed, fabricated, and placed inside the hub to sense the total unsteady rotor axial force. The two-layer transducer possesses a lower impedance than a one-layer transducer of the same thickness, i.e., the same sensitivity. A lower impedance reduces the response of the two-layer transducer to the magnetic field force inside the fan motor. The coherent output power spectrum and the complex coherence function for the unsteady rotor force and the fan noise shown that the unsteady blade force dominates the discrete- frequency noise not only at the

harmonics of the BPF but at the BPF also. The broadband noise is weakly correlated to the unsteady blade loading. The slope in the phase diagram of the complex coherence function is indicative of the time delay for the sound propagation from the fan to the microphone. The phase information was used to verify that the measured noise is indeed correlated to the unsteady blade force and not an artifact of correlating two sinusoids together.

The unsteady force on the blade is due primarily to its operation in the time invariant, spatially non-uniform inflow. In order to reduce the unsteady blade force and resulting radiated noise, an understanding of rotor non-uniform inflow fields is necessary. An experimental method of measuring the three-dimensional time invariant inflow is demonstrated. The spatially non-uniform inflow fields of a Patriot fan for cases with and without a cylinder in the inlet were measured using miniature five-hole pressure probes. The pressure outputs from such probes are related to the axial, tangential, and radial velocity vectors. Results show that the maximum axial inflow velocity occurs in the region near the shroud. The inflow in the region near the blade root is accelerated by the hub. The maximum downstream cylinder wake length occurred when the cylinder was placed symmetrically in front of the fan. The discrete-frequency radiated noise was at its maximum during this condition. The wake width is a function of radial position. The maximum wake width occurs around 0.7 rotor tip radius. The wake width decays in the regions close to the shroud and the hub due to three-dimensional and viscous effects. Fourier decomposition of the inflow velocity data was coupled with a

two-dimensional, unsteady airfoil theory to give information on the unsteady rotor force harmonic levels at the BPF and harmonics. The predicted discrete-frequency noise level was then computed using the simplified Curle's equation. The predicted and measured noise levels agreed well at the BPF and the first harmonic while the fan was behaving more like a compact source.

Design modifications and acoustic evaluation of the fan inlet and finger guard were conducted. During the evaluation, synchronous time averaging was used to enhance discrete-frequency noise while suppressing as much broadband noise as possible. The design modification of the duct inlet and finger guard were based on Washburn's recommendations [18]. The acoustic evaluation showed that the additional baffle does not reduce the fan noise. Since the discrete-frequency radiated noise is proportional to the time rate of change of the unsteady blade force, it is desirable that the radial members of the finger guard cross the blade leading edge at a large angle and pass by only a small portion of the blade leading edge at any one time. This means that the radial members should be leaned. The original factory-designed finger guard attempts to accomplish this and is certainly one of the optimal designs. However, the center plate of the original finger guard blocks the inflow and generates some noise. It is suggested that the center plate be replaced by non-intrusive circular members.

## 5.2 Recommendations

The discrete-frequency noise can be reduced by either reducing inflow distortions, avoiding Blade tip interaction with the shroud boundary layer, or redesigning the blades to reduce the blade-rate force. For the Patriot fan, since an optimum inlet and finger guard design for reducing the interaction between blades and non-uniform inflow has been achieved, the optimization of tip clearance or redesign of the blades themselves are alternative approaches for reducing the discrete-frequency noise.

Significant fan noise arises from the tip region of the blades [31]. If tip clearance is large, the leakage of air through the clearance is significant and the leakage vortex formed in the tip region will cause significant noise. Reduction of tip clearance can improve the flow field within the shroud, increase the total pressure rise and blade loading and therefore, increase the fan efficiency and reduce the radiated discrete-frequency and broadband noise [32, 33]. It is recommended for future research that the effect of reducing the blade tip clearance in decreasing the discrete-frequency noise for the Patriot fan be evaluated.

Non-uniform distribution of tip clearance (circumferentially) can cause discrete-frequency noise at the BPF and its harmonics [34]. In this study, the flow velocity in the region near the blade tip and shroud was not measured because the probes are too large to be placed in this region. It is recommended that a flow visualization technique be applied to investigate the flow field in this region. The

circumferential distribution of tip clearance and the flow interaction due to the shroud and blade tip can be examined. The mechanisms for the generation of discrete-frequency noise in the Patriot fan can then be studied more completely.

Mechanical resonances of the blades can be an important factor in generating unsteady blade forces. They can amplify the unsteady blade force originating from the interaction of flow and blades. It is desired that none of the blade resonance frequencies coincide with the BPF or its harmonics. Resonance frequencies can be shifted, if necessary, by changing the rigidity of the blades. It was found that one blade resonance frequency of the Patriot fan occurred at 580 Hz which is fairly close to the first harmonic (573.5 Hz) of the BPF. An extensive study on the dynamic characteristic of the blade will be helpful in understanding the effect of blade resonance on the discrete-frequency noise.

# BIBLIOGRAPHY


1. Sharland, I. J., "Sources of Noise in Axial Flow Fans," J. Sound and Vibration, 1, pp. 302-322 (1964).
2. Yudin, E. Y., "On the Vortex Sound From Rotating Rods," NACA TM 1136, 1947, National Advisory Committee for Aeronautics, Washington, DC.
3. Goehlick, E., "Sound Radiation of Fans and Air Handling Installations," Fans, B. Eck, Ed. (pergamen press. Oxford, 1973), Chapt. 22, pp. 499-540.
4. Filleul, N. Le S., "An Investigation of Axial Flow Fan Noise," Sound and Vibration, 3,2, pp. 147-165 (March 1965).
5. Siddon, T. E., L. J. Leggot, "Blade Load Modulation as A Source of Discrete Frequency Fan Noise," Proceedings of Inter-Noise 73, pp. 176-185 (August 1973).
6. Hanson, D. B., "Spectrum of Rotor Noise Caused by Atmospheric Turbulence," J. Acoust. Soc. Amer., 56, pp. 110-126 (1974).
7. Rao, G. V. R., W. T. Chu, and B. K. Hodder, "Rotor Noise Due to Inflow Turbulence," AIAA Paper No. 73-632 (July 1973).
8. Mani, R., "Noise Due to the Interaction of Inlet Turbulence with Isolated Stators and Rotors," J. Sound and Vibration, 17, pp. 251-260 (1971).
9. Kryter, K. D., K. S. Pearson, "Judged Noisiness of A Band of Random Noise Containing an Audible Pure Tone," J. Acoust. Soc. Am., 38, pp. 106-112 (1965).

10. Baade, P. K., "Effects of Acoustic Loading on Acial Flow Fan Noise Generation," Noise Control Engineering, 8, 1, pp. 5-15 (Jan.- Feb., 1977).

11. Wright, S. E., "Sound Radiation from A Lifting Rotor Generated by Asymmetric Disk Loading," J. of Sound and Vibration, 9(2), pp. 223-240 (1969).

12. Clark, P. J. F., H. S. Ribiner, "Direct Correlation of Fluctuating Lift with Radiated Sound for An Airfoil in Turbulent Flow," J. Acoust. Soc. Am., 46, pp. 802-805 (1969).

13. Hersh, A. S., D. A. Bies, and W. C. Meecham, "Investigation of Aerodynamic Sound Radiation from Small Airfoils," J. Acoust. Soc. Am., 50, p. 121 (A) (1971).

14. Wright, S. E., "Discrete Radiation from Rotating Periodic Sources," J. of Sound and Vibration, Vol. 17, pp. 437-498 (1971).

15. Gutin, L., "On the Sound Field of A Rotating Aircrew," NACA Tech. Memo 1195 (1948) (Translation).

16. Fitzgerald, J. M., "Discrete Frequency Noise and Its Reduction in Small Axial Flow Cooling Fans," M.S. Thesis in Acoustics, The Pennsylvania State University (May 1982).

17. Fitzgerald, J. M. and G. C. Lauchle, "Reduction of Discrete Frequency Noise in Small, Subsonic Axial Flow Fans," J. Acoust. Soc. Am. 76: pp. 158-166 (1980).

18. Washburn, K. B., "Effects of Inflow Conditions on Discrete Frequency Noise Generated by Small, Axial Flow Fans," M.S. Thesis in Acoustics, The Pennsylvania State University (August 1985).

19. Rotron Incorporated, Woodstock, NY, Commercial Product Catalog.

20. Halliday, D. R. Resnick, Fundamentals of Physics, John Wiley & Sons, Inc., 1981, pp. 490.

21. Treaster, A. L., A. M. Yocum, "The Calibration and Application of Five-Hole Probe," Institution Society Am. Transactions, Vol. 18, No. 3, PP. 23-34 (1979).

22. Zierke, W. C., Applied Research Lab., The Penn State University, Private Communication.

23. Neumann, H., H. Yeh, "Lift and Pressure Fluctuations of a Cambered Airfoil Under periodic Gusts and Applications in Turbomachinery," Trans. ASME, J. Engr. Power (January 1973).

24. Sears, W. R., "Some Aspects of Non-Stationary Airfoil Theory and Its Practical Application," J. Aero. Sci. (1941).

25. Horlock, J. H., "Fluctuating Lift Forces on Aerofoils Moving Through Transverse and Chordwise Gusts," Trans. ASME, J. Basic Eng., Paper No. 68-FE-28 (1968).

26. Curle, N., "The Influence of Solid Boundaries Upon Aerodynamic Sound," Proc. Roy. Soc. (London) Ser. A231, pp. 504-514 (1955).

27. Lighthill, M. J., "Sound Generated Aerodynamically," Proc. Roy. Soc. (London) Ser. A267, pp. 147-182 (1962).

28. Sidden, T. E., "Surface Dipole Strength by Cross-Correlation Method," J. Acoust. Soc. Am., 53, pp. 613-633 (1973).

29. Clark, P. J. F., H. S. Ribner, "Direct Correlation of Fluctuating Lift with Radiated Sound For An Airfoil in Turbulent Flow," J. Acoust. Soc. Am., 46, pp. 802-805 (1969).

30. Gray, L. M., "A Review of the Physics of Axial Fan Acoustics and Aerodynamics with a View Toward Noise Control," Proc. Noise-Con 83, pp. 187-196.

31. Schlinker, R. H., R. K. Amiet, "Rotor-Vortex Interaction Noise," NASA-CR-3744 (Oct. 1983).

32. Fukano, T., Y. Kodama, and Y. Senoo, "Noise Generated by Low Pressure Axial Flow Fan, I: Modeling of the Turbulent Noise," J. of Sound and Vibration, 50, pp. 63-74 (1977).

33. Lakshminarayana, B., "Methods of Predicting the Tip Clearance Effects in Axial Flow Turbomachienry," Transactions of the American Society of Mechanical Engineers, 92, pp. 467-482 (1970).

34. Fukano, T., Y. Takamatsu, "The Effects of Tip Clearance on the Noise of Low Pressure Axial and Mixed Flow Fans," J. of Sound and Vibration, 105(2), pp. 291-308 (1986).

END
DATE
9-88
DTIC